Molecular Therapy
Original Article

lncRNA SNHG11 Promotes Gastric Cancer Progression by Activating the Wnt/β-Catenin Pathway and Oncogenic Autophagy

Qiong Wu,[1] Jiali Ma,[1] Jue Wei,[1] Wenying Meng,[1] Yugang Wang,[1] and Min Shi[1]

[1]Department of Gastroenterology, Tongren Hospital, Shanghai Jiao Tong University School of Medicine, 1111 Xianxia Road, Shanghai 200336, China

Long non-coding RNAs (lncRNAs) are under active investigation in the development of cancers, including gastric cancer (GC). Oncogenic autophagy is required for cancer cell survival. The present study aimed to investigate the regulatory role of lncRNA small nucleolar host gene 11 (SNHG11) in GC. We show that SNHG11 is upregulated in GC, and that its upregulation correlated with dismal patient outcomes. Functionally, SNHG11 aggravated oncogenic autophagy to facilitate cell proliferation, stemness, migration, invasion, and epithelial-to-mesenchymal transition (EMT) in GC. Mechanistically, SNHG11 post-transcriptionally upregulated catenin beta 1 (CTNNB1) and autophagy related 12 (ATG12) through miR-483-3p/miR-1276, while the processing of precursor (pre-) miR-483/pre-miR-1276 was hindered by SNHG11. SNHG11 induced GSK-3β ubiquitination through interacting with Cullin 4A (CUL4A) to further activate the Wnt/β-catenin pathway. Intriguingly, SNHG11 regulated autophagy in a manner dependent on ATG12 rather than the Wnt/β-catenin pathway, whereas SNHG11 contributed to the malignant behaviors of GC cells via both pathways. Finally, SNHG11 upregulation in GC cells was shown to be transcriptionally induced by TCF7L2. In conclusion, we reveal that SNHG11 is an onco-lncRNA in GC and might be a promising prognostic and therapeutic target for GC.

INTRODUCTION

Globally, gastric cancer (GC) is the fourth most common malignancy and the second major cause of cancer-related deaths.[1,2] The high mortality of GC is mainly attributed to tumor metastasis, tumor recurrence, and treatment resistance.[3] Unfortunately, diagnostic and therapeutic methods still need to be further developed before achieving a significant improvement on the prognosis of GC patients at the advanced stage.[4,5] Therefore, it is necessary to further understand the key molecular events behind GC development and metastasis.

Long non-coding RNAs (lncRNAs) are RNA transcripts with a sequence of greater than 200 nt and without protein-coding function.[6] Numerous studies have shown that lncRNAs could affect a wide spectrum of biological behaviors in tumor cells, such as cell proliferation,[7] apoptosis,[8] stemness,[9] metastasis,[10] and autophagy.[11] lncRNAs fulfill their tumor-driving or tumor-repressing functions in cancer cells by dysregulating certain genes, and the underlying mechanism varies depending on their subcellular localization and interaction with different biomolecules.[12] So far, the association between lncRNAs and carcinogenesis and metastasis in GC has been well established based on multiple studies.[13,14] Small nucleolar host gene 11 (SNHG11) is a newly identified lncRNA that has been suggested as a prognostic marker in prostate cancer and ovarian cancer.[15,16] Additionally, a study has also indicated the upregulation of SNHG11 in pancreatic cancer.[17] However, the relationship of SNHG11 to GC development remains unknown.

Autophagy is a cellular self-degradative process responding to various cellular stresses such as hypoxia and starvation. During this process, cytoplasm, organelles, and cellular proteins are engulfed, digested, and then recycled, so that cellular metabolism is sustained.[18,19] On the one hand, autophagy has been proven to suppress the growth of primary tumors in genetically engineered mouse models,[20,21] On the other hand, autophagy has been demonstrated to be required for the maintenance and progression of tumors.[22,23] Cytoprotective autophagy functions as a survival mechanism under nutrient starvation conditions. When extracellular nutrient supplies are sufficient to support cellular metabolism, the cytopreotective function of autophagy is attenuated and the effects on facilitating cell death are augmented.[24] Notably, although autophagy is thought to mediate the balance between cell survival and death, more evidence supports the role of autophagy in cell survival.[19] Particularly, substantial reports indicate that autophagy contributes to the survival and maintenance of tumor cells in response to metabolic stress *in vitro*, as well as in hypoxic tumor regions *in vivo*.[24–28] Besides the regulation on cell survival, recent studies have revealed that autophagy also aggravates metastasis by influencing anoikis resistance, cell migration and

Received 15 September 2019; accepted 8 October 2020;
https://doi.org/10.1016/j.ymthe.2020.10.011.

Correspondence: Yugang Wang, Department of Gastroenterology, Tongren Hospital, Shanghai Jiao Tong University School of Medicine, 1111 Xianxia Road, Shanghai 200336, China.
E-mail: wyg0061@shtrhospital.com
Correspondence: Min Shi, Department of Gastroenterology, Tongren Hospital, Shanghai Jiao Tong University School of Medicine, 1111 Xianxia Road, Shanghai 200336, China.
E-mail: sm1790@shtrhospital.com

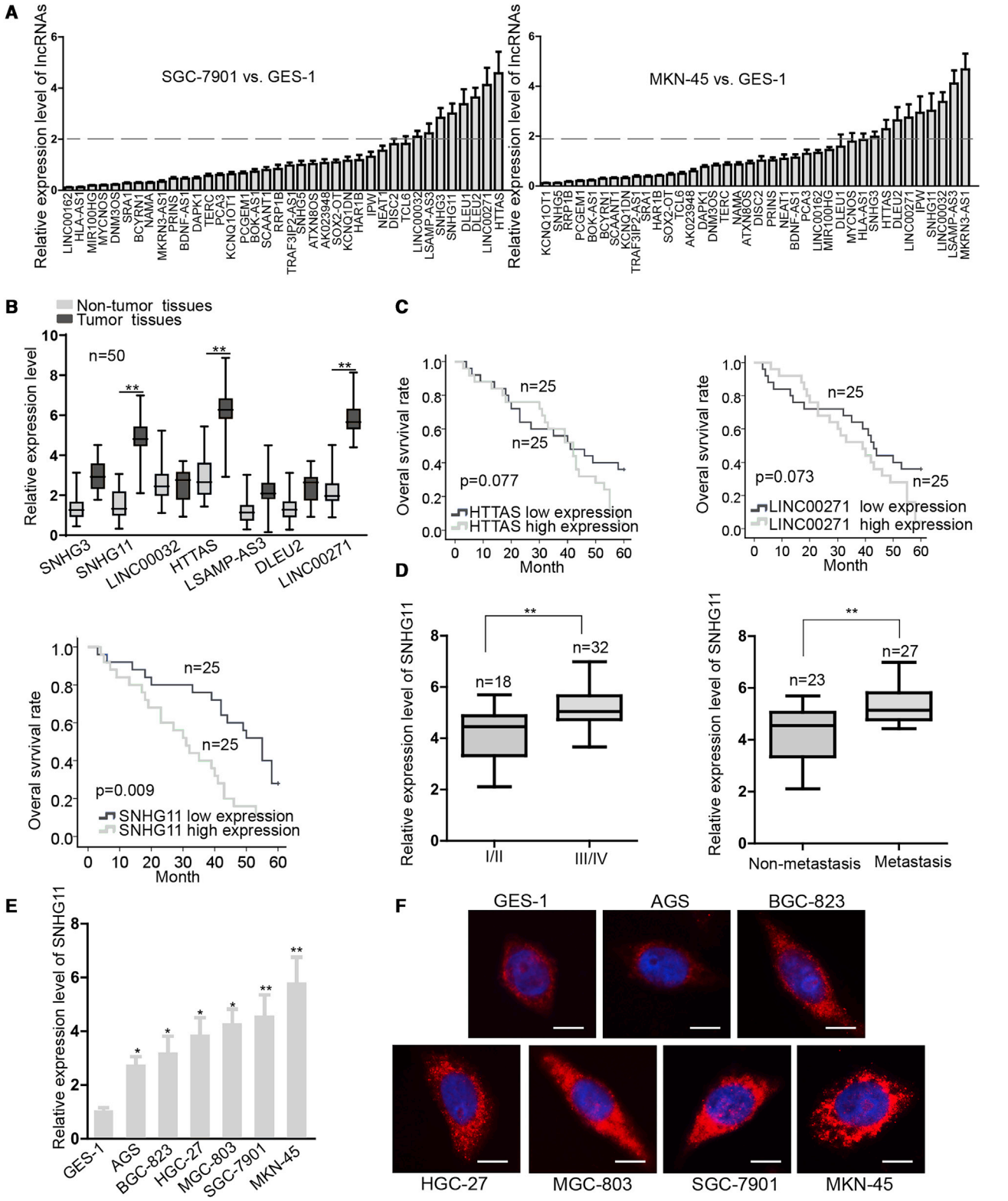

(legend on next page)

invasion, and epithelial-to-mesenchymal transition (EMT) progression.[29] Moreover, the oncogenic autophagy in GC has been evidenced by a number of studies. For example, autophagy protects GC cells from vincristine-induced apoptosis.[30] The miR-423-3p-Bim axis activates oncogenic autophagy to accelerate GC progression.[31] However, it is unclear whether SNHG11 regulates autophagy during GC development.

The canonical Wnt/β-catenin pathway is widely acknowledged as an oncogenic signaling that regulates cell survival, stemness, and metastasis in diverse carcinomas.[32–34] Its activation is characterized by cytoplasmic accumulation and nuclear translocation of β-catenin, followed by the formation of complexes with transcription factors like TCF7L2 and LEF1, eventually inducing the target genes such as EMT-related genes.[35,36] Mounting studies have suggested the implications of Wnt/β-catenin pathway for the carcinogenesis of cancers including GC.[37,38] However, the relationship between SNHG11 and Wnt/β-catenin signaling in GC remains to be investigated.

RESULTS

Expression Pattern and Prognostic Significance of SNHG11 in GC

To identify the lncRNAs related to GC development, we applied a lncRNA PCR array to test the level of 38 lncRNAs identified by a previous study in two GC cell lines (SGC-7901 and MKN-45) relative to the normal gastric epithelial cells (GES-1) (Figure S1A). Among them, eight lncRNAs were upregulated with the fold change >2 in SGC-7901 cells while nine lncRNAs were upregulated in MKN-45 cells when compared to GES-1 cells, and seven lncRNAs (including LINC00032, LSAMP-AS3, SNHG3, SNHG11, DLEU2, LINC00271, and HTTAS) were shared in the above two GC cell lines (Figure 1A). Additionally, quantitative real-time RT-PCR analysis revealed that HTTAS, LINC00271, and SNHG11 were significantly upregulated in 50 GC tissues compared with matched non-tumor tissues (Figure 1B). To further narrow our selection, the prognostic values of these three lncRNAs were assessed in GC patients. The results of Kaplan-Meier analysis depicted that a high SNHG11 level predicted poor overall survival in GC patients ($p = 0.009$) (Figure 1C). In addition, tissues from GC patients at an advanced stage or with metastasis expressed a higher SNHG11 level than did the corresponding controls (Figure 1D). Therefore, we conducted a further investigation on the role of SNHG11 in GC. Also, we verified through quantitative real-time RT-PCR that the SNHG11 level was elevated in six GC cell lines (AGS, BGC-823, HGC-27, MGC-803, SGC-7901, and MKN45) compared to the normal GES-1 cells (Figure 1E). Moreover, the outcomes of fluorescence *in situ* hybridization (FISH) staining of SNHG11 validated the strong fluorescence intensity of SNHG11 in GC cells versus the normal GES-1 cells, and they indicated that SNHG11 was mainly distributed in the cytoplasm of all of these cells (Figures 1F and S1B). In addition, the UCSC genome browser (http://genome.ucsc.edu/) revealed that SNHG11 has two homologous small nucleolar RNAs (snoRNAs), ACA39 and ACA60. We verified that the expression levels of both snoRNAs presented no significant difference between GC tissues and paired non-tumor ones (Figure S1C), excluding the potential participation of them in GC progression. These results indicated that SNHG11 upregulated in GC might participate in tumor progression and metastasis, and its elevation led to poor prognosis of GC patients.

Inhibiting SNHG11 Hampers the Proliferative Ability and the Stem Cell Properties of GC Cells *In Vitro*

Next, to detect the impact of SNHG11 on cell proliferation and stemness, we designed loss-of-function assays in two GC cell lines (SGC-7901 and MKN-45) expressing high SNHG11 levels. Quantitative real-time RT-PCR data confirmed the significant knockdown of SNHG11 in both cells, and that short hairpin RNA (shRNA) (sh)/SNHG11#1/2 presented higher knockdown efficiency than did sh/SNHG11#3 (Figure 2A). We also confirmed the efficient depletion of SNHG11 by sh/SNHG11#1/2 in two GC cells via FISH staining, as evidenced by the significant weakening of SNHG11 fluorescence intensity under the respective transfection of the two shRNAs (Figure S2A). Then, we found that the viability and clonogenic capability of GC cells were attenuated by sh/SNHG11#1/2 transfection (Figures 2B, 2C, S2B, and S2C). Likewise, the number of 5-ethynyl-2′-deoxyuridine (EdU)-positive GC cells decreased upon SNHG11 knockdown (Figures 2D and S2D). Since cancer cells are able to acquire stem cell properties that contribute to tumorigenesis, invasive growth, and metastasis,[39,40] we then probed the influence of SNHG11 on the stemness of GC cells. As expected, knockdown of SNHG11 impeded the sphere formation capacity of GC cells (Figure 2E). According to the results of flow cytometry analysis, the population of $CD133^+$ GC cells was reduced due to SNHG11 knockdown (Figure 2F). Moreover, the protein levels of stemness-related genes were also reduced by silenced SNHG11 in GC cells, including Twist, Nanog, OCT4, LGR5, EpCAM, CD133, and SOX2 (Figure 2G). Additionally, although a few studies have argued that β-actin, the loading control we applied here, is highly expressed in GC samples,[41,42] we verified that it presents no significant change between GC tissues and paired non-cancerous ones collected in this study (Figure S2E), which validated that β-actin was allowed to be used as a loading control here. Furthermore, we identified that the fluorescence intensities of both SNHG11 and the stemness marker ALDH1 were higher in the tumor spheres derived

Figure 1. SNHG11 Is Upregulated in GC and Indicates Poor Prognosis of GC Patients

(A) Quantitative real-time RT-PCR was applied to detect the level of 38 lncRNAs in GC cells (GSC-7901 and MKN-45) relative to normal gastric epithelial cells (GES-1). (B) Expressions of the selected seven lncRNAs in GC tissues and paired adjacent normal tissues were detected by quantitative real-time RT-PCR. (C) Association of HTTAS, LINC00271, and SNHG11 with the prognosis of 50 GC patients was determined by Kaplan-Meier analysis and a log-rank test. (D) Expression of SNHG11 in tissues from GC patients at different stages (stages I/II and III/IV) or with metastasis or not (non-metastasis and metastasis) was determined by quantitative real-time RT-PCR. (E) SNHG11 expression in six GC cell lines (AGS, BGC-823, HGC-27, MGC-803, SGC-7901, and MKN-45) and normal GES-1 cells was determined by quantitative real-time RT-PCR. (F) FISH staining of SNHG11 in six GC cell lines and GES-1 cells. Scale bars, 10 μm. Error bar denotes SD. *$p < 0.05$, **$p < 0.01$.

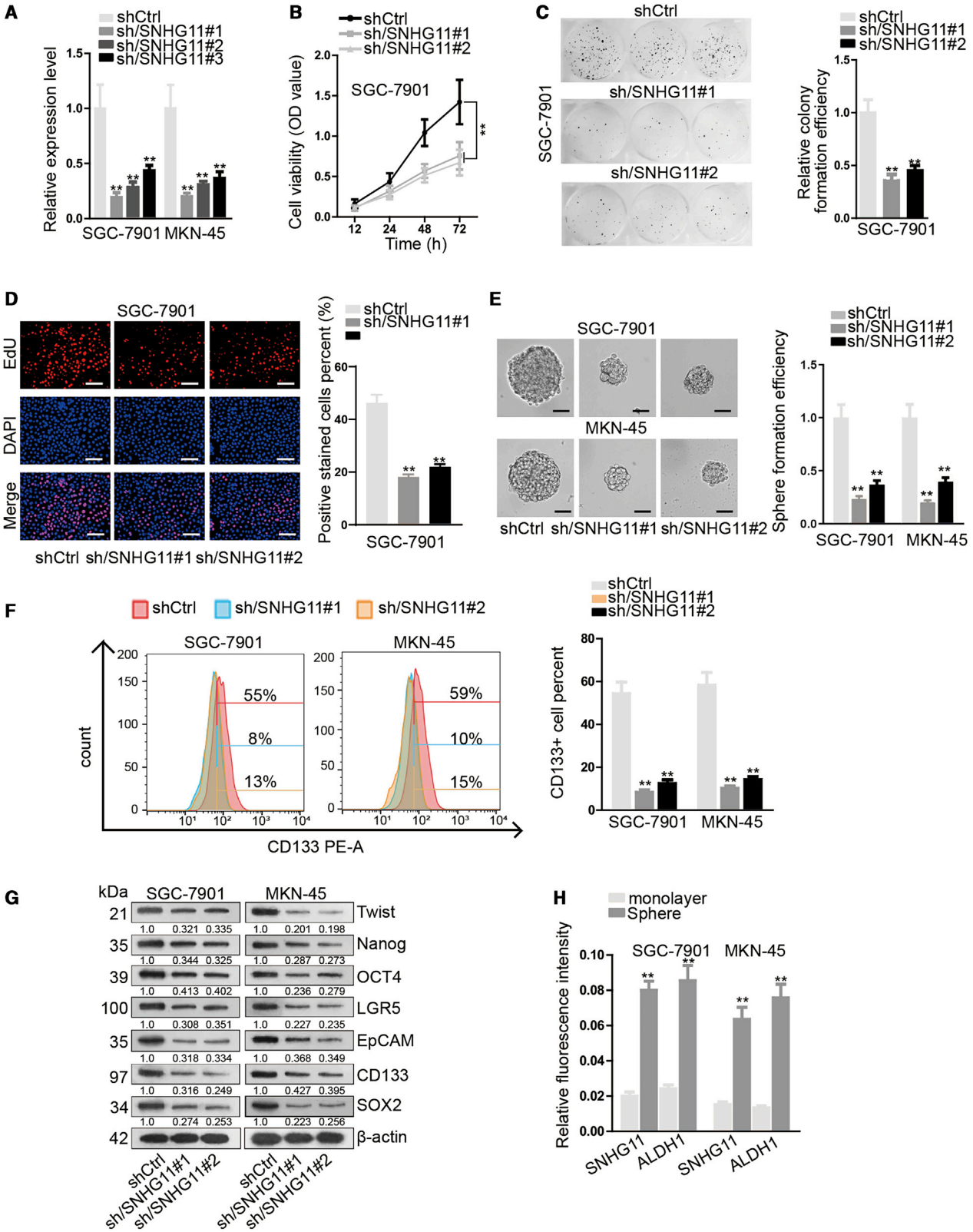

(legend on next page)

from GC cells than in the monolayer of GC cells (Figures 2H and S2F). The above data suggested that losing SNHG11 hampers cell proliferation and stemness in GC *in vitro*.

Silencing SNHG11 Hinders Cell Migration and Invasion and EMT by Inhibiting Autophagy in GC

Then, the influence of SNHG11 on *in vitro* GC metastasis was investigated. Through transwell assays, we observed that the absence of SNHG11 prevented the migration and invasion of GC cells (Figures 3A and S3A). Immunofluorescence (IF) staining and western blot analysis confirmed the increased E-cadherin level and the decreased N-cadherin, MMP2, and MMP7 levels in GC cells responding to the deficiency of SNHG11 (Figures 3B, S3B, and 3BC), indicating that SNHG11 knockdown hampers EMT in GC cells. Moreover, cancer metastasis is a multistep process during which cancer cells possessing anoikis resistance and less adhesion to the extracellular matrix or to neighboring cells metastasize to and grow in other tissues.[43–45] The results of the cell-matrix adhesion assay revealed that knocking down SNHG11 strengthened the adhesion of GC cells to matrix (Figure 3C). Additionally, we detected the effect of SNHG11 on the anoikis resistance of GC cells. GC cells were cultured in the culture dishes pre-coated with poly(2-hydroxyethyl methacrylate) (poly-HEMA), and the apoptosis-related genes were detected by western blot at 12, 24, and 48 h after suspension.[43,46] Data showed that the levels of pro-apoptotic Bax and ITGB1 were induced, whereas the level of anti-apoptotic Bcl-2 was reduced at 12, 24, and 48 h in GC cells with SNHG11 knockdown (Figure 3D), indicating that downregulating SNHG11 attenuated anoikis resistance of GC cells. Later, we found that the apoptosis of GC cells was facilitated under the knockdown of SNHG11 (Figures 3E and S3D). Consistently, the level of Bcl-2 was decreased, whereas the levels of cleaved caspase-3, cleaved caspase-6, and cleaved poly(ADP-ribose) polymerase (PARP) were increased upon SNHG11 knockdown (Figure 3F).

It has been documented that autophagy can influence cell viability, differentiation, anoikis resistance, migration, invasion, EMT progression, as well as tumor cell dormancy.[29] However, it has also been stated that autophagy can exert either a survival-supporting or death-promoting function in cancer cells.[47] In this study, we wanted to determine the role of autophagy in GC. We found that compared with GES-1 cells, GC cells (SGC-7901 and MKN-45) presented much increased intensities of LC3-II during starvation (Figure S4A). Then, SGC-7091 and MKN-45 cells were treated with bafilomycin A1 (BafA1) to inhibit the merge of autophagosomes and lysosomes, thereby preventing autophagy. Consequently, cell viability, migration, and invasion were all inhibited after the treatment with BafA1 (Figures S4B and S4C). Also, inhibiting autophagy by BafA1 led to increased levels of E-cadherin and decreased levels of N-cadherin, MMP2, MMP7, and Twist in GC cells (Figure S4D). These data corroborated that autophagy facilitates cell survival, migration, invasion, and EMT in GC. Thereafter, we detected whether SNHG11 affected autophagy in GC cells. As proved by the results of IF staining, knockdown of SNHG11 reduced LC3 dots in GC cells (Figures 3G and S4E). Moreover, to further observe autophagy flux, GC cells were transfected with GFP-monomeric red fluorescent protein (mRFP)-LC3. As a result, SNHG11 inhibition reduced both red and yellow puncta in GC cells, while the treatment with rapamycin (Rapa) but not BafA1 rescued such reduction; additionally, BafA1 treatment alone reduced red puncta, and treatment of Rapa alone increased both red and yellow puncta (Figures 3H and S4F). Furthermore, western blot results revealed that the loss of SNHG11 decreased the ratio of LC3-II/LC3-I and the level of LAMP1, and increased the level of p62 in GC cells (Figure 3I), while LAMP1 was the key regulator in promoting the fusion of autophagosomes and lysosomes.[48] Hence, we discovered that SNHG11 positively regulates autophagy in GC cells. Taken together, these data suggested that SNHG11 knockdown restrains cell migration, invasion, and EMT, but induces cell apoptosis in GC by inhibiting autophagy.

SNHG11 Overexpression Triggers the Proliferation, Stemness, Migration, Invasion, and Autophagy of Normal GES-1 Cells and GC Cells *In Vitro*

Subsequently, we overexpressed SNHG11 by pcDNA3.1/SNHG11 in AGS cells, which expressed a relatively low SNHG11 level among the six detected GC cell lines, and in normal GES-1 cells as well. Quantitative real-time RT-PCR data validated the pronounced upregulation of SNHG11 in these cells after transfecting pcDNA3.1/SNHG11 versus the empty pcDNA3.1 vector (Figure S5A). Consequently, the proliferation of GES-1 and AGS cells was aggravated under SNHG11 overexpression (Figures S5B and S5C). Similarly, GES-1 and AGS cells with overexpressed SNHG11 exhibited enhanced sphere formation efficiency and $CD133^+$ ratio (Figures S5D and S5E). Also, the levels of stemness-associated genes, including Twist, Nanog, OCT4, LGR5, EpCAM, CD133, and SOX2, were increased in these two kinds of cells under SNHG11 upregulation (Figure S5F). These data indicated that ectopic expression of SNHG11 not only enhanced the stemness of GC cells, but also helped normal gastric cells to acquire stem cell-like characteristics. Additionally, the abilities of AGS and GES-1 cells to migrate and invade were facilitated upon SNHG11 overexpression (Figure S5G). Accordingly, the level of

Figure 2. SNHG11 Positively Regulates Cell Proliferation and Stemness in GC *In Vitro*

(A) Knockdown of SNHG11 by three shRNAs in SGC-7901 and MKN-45 cells was confirmed by quantitative real-time RT-PCR analysis. (B) A CCK-8 assay was applied to detect cell viability at indicated time points in SGC-7901 cells transfected with shCtrl, sh/SNHG11#1, or sh/SNHG11#2. (C) Representative images and quantification of colony formation efficiency of SGC-7901 cells with indicated transfections. (D) Representative images and quantification of EdU^+ cell percent in SGC-7901 cells with indicated transfections. Scale bars, 50 μm. (E) Images of tumor spheres formed by two GC cell lines and the quantity of sphere formation efficiency. Scale bars, 100 μm. (F) Flow cytometry analysis was applied to detect $CD133^+$ GC cells under SNHG11 knockdown. (G) Western blots of stemness markers in GC cells transfected with shCtrl, sh/SNHG11#1, or sh/SNHG11#2. (H) Quantification of the fluorescence intensity of SNHG11 assayed by FISH and the fluorescence intensity of stemness marker ALDH1 assayed by IF in a monolayer of GC cells or the tumor sphere formed by GC cells. Error bar denotes SD. $^{**}p < 0.01$.

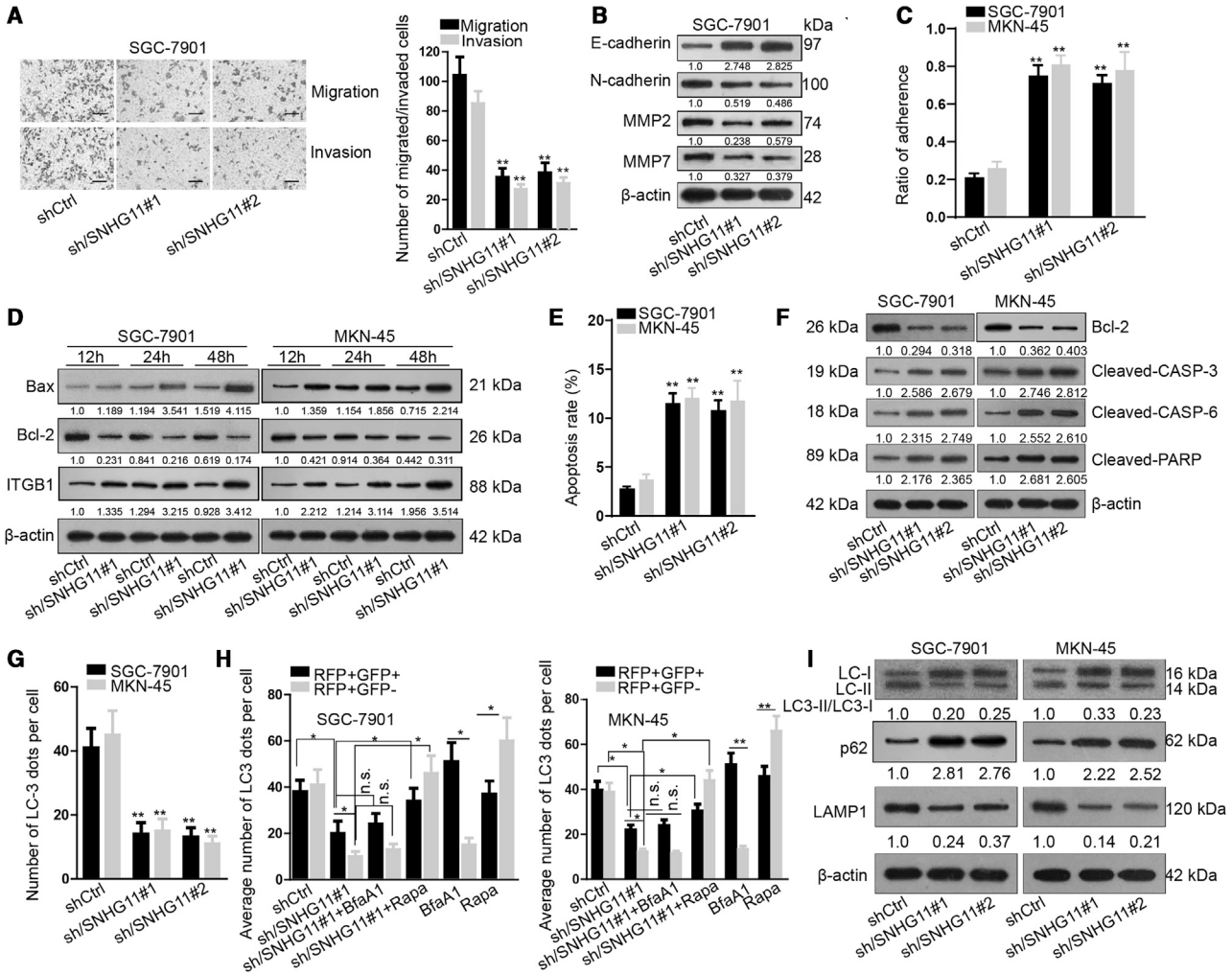

Figure 3. SNHG11 Facilitates Metastasis and Autophagy in GC Cells

(A) The invasion and migration abilities of GC cells under SNHG11 knockdown were monitored through a transwell system with or without Matrigel. Scale bars, 100 μm. (B) Western blots of EMT markers (E-cadherin, N-cadherin, MMP2, and MMP7) in SGC-7901 cells. (C) Matrix adhesion assay of SGC-7901 and MKN-45 cells at 90 min under the knockdown of SNHG11. (D) Western blots of Bax, Bcl-2, and ITGB1 in GC cells upon the pre-treatment of anoikis assay. (E) Quantification of apoptotic ratio according to flow cytometry analysis of GC cells upon SNHG11 knockdown. (F) Western blots of Bcl-2, cleaved caspase-3, cleaved caspase-6, and cleaved PARP in GC cells under SNHG11 knockdown. (G) Quantification of endogenous LC3 dots assessed by IF staining in SGC-7901 and MKN-45 cells during starvation at 24 h following the transfection of shCtrl, sh/SNHG11#1, or sh/SNHG11#2. (H) Numbers of acidified autophagosomes ($GFP^{-}RFP^{+}$) (red) compared to neutral autophagosomes ($GFP^{+}RFP^{+}$) (yellow) per cell of each group were quantified. (I) Western blots of autophagy-related proteins (LC3-II/LC3-I, p62, and LAMP1) in GC cells under SNHG11 knockdown. Error bar denotes SD. *$p < 0.05$, **$p < 0.01$. n.s., not significant.

E-cadherin declined, while the levels of N-cadherin, MMP2, and MMP7 were augmented in these cells under SNHG11 upregulation (Figure S5H). In addition, their ability of adhesion to matrix was weakened by upregulated SNHG11 (Figure S5I). These data suggested that SNHG11 overexpression facilitated the metastasis of GC cells as well as the normal GES-1 cells *in vitro*. Additionally, we observed the increase of LC3 dots, elevation of the LC3-II/LC3-I ratio and LAMP1 level, and reduction of the p62 level in GES-1 and AGS cells after SNHG11 overexpression (Figures S5J and S5K). In summary, the abovementioned data indicated that SNHG11 overexpression triggers the proliferation, stemness, migration, invasion, and autophagy of normal GES-1 cells and GC cells *in vitro*.

SNHG11 Induces the Wnt/β-Catenin Pathway to Regulate GC Progression and Metastasis, but Not Autophagy

We then proceeded to investigate the regulatory mechanism of SNHG11 in GC. First, we detected the effect of SNHG11 on several well-known signaling pathways responsible for cancer progression, including the Wnt/β-catenin, mitogen-activated protein kinase (MAPK), phosphatidylinositol 3-kinase (PI3K)/AKT, Hedgehog,

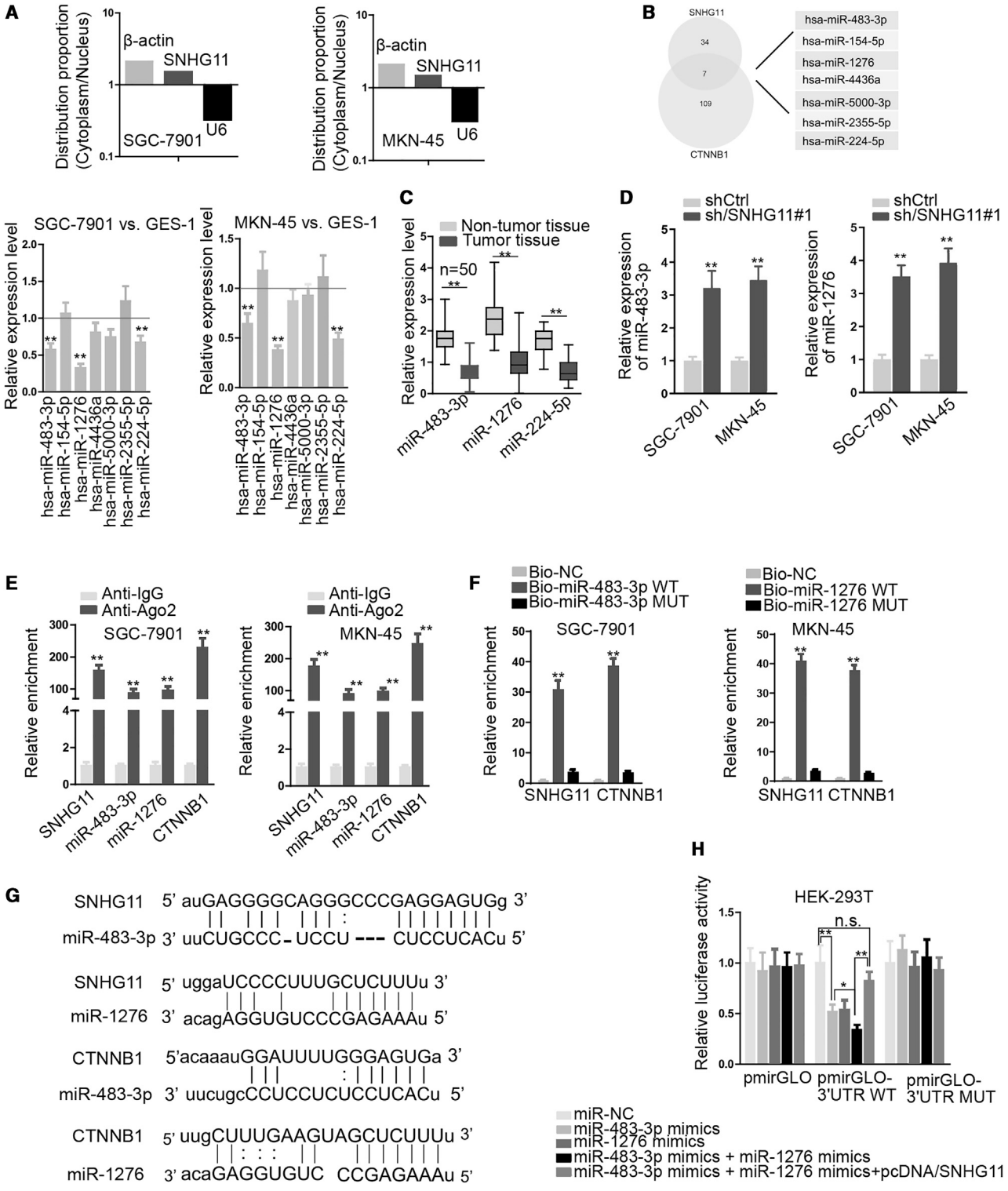

Figure 4. SNHG11 Decoys miR-483-3p and miR-1276 to Upregulate CTNNB1

(A) Cytoplasmic localization of SNHG11 was confirmed in GC cells through subcellular fractionation. (B) starBase 3.0 prediction identified seven miRNAs shared by SNHG11 and CTNNB1. Expression levels of seven miRNAs in SGC-7901 and MKN-45 cells versus GES-1 cells were determined by quantitative real-time RT-PCR. (C) Expressions of

(legend continued on next page)

and signal transducer and activator of transcription (STAT) pathways.[38,49–52] As a result, we found that knockdown of SNHG11 led to the specific downregulation of β-catenin, but had no apparent impact on the level of phosphorylated (p-)MAPK, p-PI3K, p-AKT, GLI1, GLI2, GLI3, and p-STAT3 in GC cells (Figure S6A). Then, the outcomes of the TOP/FOP flash assay confirmed that SNHG11 knockdown markedly reduced the activity of the Wnt/β-catenin pathway (Figure S6B). Also, we observed the decrease of nuclear β-catenin level in both GC cells with depleted SNHG11 (Figure S6C). The data above validated that SNHG11 positively regulates the Wnt/β-catenin pathway in GC.

Later, we detected whether SNHG11 affects GC progression depending on the Wnt/β-catenin pathway. We discovered that silencing SNHG11 reduced cell proliferation, stemness, migration, and invasion, and EMT, while such inhibitory impacts were partly recovered after adding LiCl, which is commonly used to activate the Wnt/β-catenin pathway (Figures S6D–S6H). However, we found that the treatment with LiCl failed to reverse the reduction of LC3 dots and the inhibition on autophagy flux caused by SNHG11 knockdown in GC cells (Figures S7A and S7B). Also, LiCl treatment resulted in no evident alteration on the affected LC3-II/LC3-I ratio and LAMP1 and p62 levels in GC cells with SNHG11 knockdown (Figure S7C). These data suggested that Wnt/β-catenin is not required for the regulation of SNHG11 on autophagy in GC cells.

Knocking Down SNHG11 Impedes the Tumorigenesis and Metastasis of GC via the Wnt/β-Catenin Pathway *In Vivo*

Next, we tested whether the function of SNHG11 in GC is mediated by the Wnt/β-catenin pathway *in vivo*. We carried out xenograft transplantation in mice by subcutaneous injection of MKN-45 cells transfected with shRNA control (shCtrl) or sh/SNHG11#1. The mice injected with sh/SNHG11#1-transfected MKN-45 cells were treated without or with LiCl. We observed that sh/SNHG11#1-transfected MKN-45 cells presented a slower tumor growth rate and generated smaller and lighter tumors than did the control group, indicating that inhibiting SNHG11 suppressed *in vivo* tumor growth. Then, treatment with LiCl reversed the growth-inhibitory effect of sh/SNHG11#1 *in vivo* (Figure S7D). Importantly, the xenografts with depleted SHNG11 presented a lower staining ratio of the proliferation marker Ki67 and stemness marker CD133 in tumors, and such phenomena were also reversed after further treatment with LiCl (Figure S7E). Concordantly, the protein levels of stemness-related genes were lessened in xenografts with SNHG11 knockdown and were restored after the co-treatment of LiCl (Figure S8A). Moreover, we validated that in the xenografts with inhibited SNHG11, E-cadherin and p62 levels were increased, whereas N-cadherin, MMP2, and MMP7 levels and the LC3-II/LC3-I ratio were decreased compared to the control group, and LiCl treatment reversed the above changes induced by SNHG11 suppression (Figure S8B). In the meantime, we also performed *in vivo* metastasis experiments, and H&E staining data showed that tail vein injection of MKN-45 cells with downregulated SNHG11 in mice resulted in fewer metastatic nodes compared to the control, and such an effect of SNHG11 knockdown was reversed by LiCl treatment (Figure S8C). These results indicated that knockdown of SNHG11 hinders GC tumorigenesis and metastasis *in vivo*.

SNHG11 Upregulates CTNNB1 through miR-1276 and miR-483-3p

Since the accumulation and nuclear translocation of β-catenin are key steps in Wnt/β-catenin activation,[53] we explored the mechanism whereby SNHG11 regulates β-catenin. Subcellular location is known to be informative with regard to the regulatory function of lncRNAs.[54] Through bioinformatics prediction via lncLocator (http://www.csbio.sjtu.edu.cn/bioinf/lncLocator/), we identified that SNHG11 was mainly located in cytoplasm, and this phenomenon was further proven by the results of subcellular fractionation (Figure 4A), which are consistent with previous FISH staining outcomes (Figure 1F). Therefore, we tried to probe whether SNHG11 regulates β-catenin at the post-transcriptional level by serving as a competing endogenous RNA (ceRNA) of CTNNB1, the coding gene of β-catenin. starBase 3.0 (http://starbase.sysu.edu.cn/) predicted seven microRNAs (miRNAs) shared by SNHG11 and CTNNB1 (Figure 4B). Among them, only miR-483-3p, miR-1276, and miR-224-5p presented significant downregulation in SGC-7901 and MKN-45 cells versus GES-1 cells (Figure 4B). Additionally, the three miRNAs were also confirmed to be lowly expressed in GC tissues compared with para-tumorous tissues (Figure 4C). However, only miR-1276 and miR-483-3p were negatively correlated with SNHG11 in expression in GC samples (Figure S9A). Hence, the two miRNAs were selected for further investigation. Interestingly, we found that knocking down SNHG11 markedly elevated the expression of both miR-1276 and miR-483-3p in SGC-7901 and MKN-45 cells (Figure 4D), whereas overexpressing neither miR-1276 nor miR-483-3p altered the level of SNHG11 in the two GC cells (Figure S9B). The immunoprecipitation (IP) of SNHG11, miR-1276, miR-483-3p, and CTNNB1 by Ago2 indicated that miR-1276 and miR-483-3p potentially interacted with SNHG11 or CTNNB1 in RNA-induced silencing complexes (RISCs) (Figure 4E). Quantitative real-time RT-PCR results confirmed the enrichment of SNHG11 and CTNNB1 in the compounds pulled down by Bio-miR-483-3p wild-type (WT) and Bio-miR-1276 WT rather than by the biotin-labeled mutant (Mut) sequences (Figure 4F). In addition, the binding sequences on SNHG11 and CTNNB1 for miR-483-3p and miR-1276 are depicted in Figure 4G. Then, we discovered that respective overexpression of miR-483-3p or miR-1276 reduced the luciferase activity of the

miR-483-3p, miR-1276, and miR-224-5p in GC tissues versus matched para-tumorous tissues were examined by quantitative real-time RT-PCR. (D) Expression levels of miR-483-3p and miR-1276 in GC cells under SNHG11 knockdown were assessed by quantitative real-time RT-PCR. (E and F) Interaction of miR-483-3p and miR-1276 with SNHG11 and CTNNB1 was investigated through the RIP and pull-down assays. (G) Interacting sequences on SNHG11 and CTNNB1 for miR-483-3p and miR-1276 were predicted by starBase 3.0. (H) A luciferase reporter assay was used to determine the luciferase activity in HEK293T cells of indicated groups. Error bar denotes SD. $^{*}p < 0.05$, $^{**}p < 0.01$.

CTNNB1 3′ UTR WT reporter, and co-overexpression of them further enhanced such an effect, while such a reduction was fully recovered under the co-transfection of pcDNA3.1/SNHG11. However, the luciferase activities of empty pmirGLO reporter and CTNNB1 mutant reporter (with both miR-483-3p and miR-1276 sites mutated) presented no significant changes (Figure 4H). Furthermore, quantitative real-time RT-PCR data demonstrated that knockdown of SNHG11 reduced the CTNNB1 level, while such an effect was partially reversed by respective inhibition of miR-1276 or miR-483-3p and fully recovered when co-inhibiting both of them (Figure S9C). Also, we verified that in GC tissues, CTNNB1 was negatively correlated with miR-483-3p and miR-1276 and positively correlated with SNHG11 (Figure S9D). Collectively, it was suggested that SNHG11 enhances CTNNB1 expression in GC through miR-1276 and miR-483-3p.

SNHG11 Inhibits miR-1276 and miR-483-3p by Inhibiting Their Pre-miRNA Processing

Previously, we have found that besides acting as the sponge of miR-1276 and miR-483-3p, SNHG11 also negatively affects their expressions in GC cells. Hence, we tried to explore the underlying mechanism for the next step. A former study showed that a cytoplasmic lncRNA can interact with pre-miRNAs at the DICER splice cleavage sites to influence pre-miRNA processing, thus affecting the level of mature miRNA.[55] As expected, we found that depletion of SNHG11 resulted in increased levels of pre-miR-1276 and pre-miR-483 in two GC cell lines (Figure S10A). Importantly, we found that SNHG11 contained sequences complementary to the DICER cleavage sites on pre-miR-1276 and pre-miR-483, with a free energy of −9.4 kcal/mol for SNHG11 binding to pre-miR-1276 and −12 kcal/mol for the binding to pre-miR-483 (Figure S10B). We then showed that only the SNHG11 biotin probe could pull down pre-miR-483 and pre-miR-1276 in GC cells, while the biotinylated sequence with mutant binding sites for pre-miR-483 or pre-miR-1276 lost such function (Figure S10C). It is known that the positioning loop within the RNase III domains of DICER is important for cleavage of the pre-miRNA 3′ arm and 5′ arm, and that TRBP forms a complex with DICER to regulate the recruitment of the pre-miRNA 3′ end to the PAZ domain of DICER.[56,57] After validating the binding of SNHG11 to the loop region of pre-miR-1276 and pre-miR-483, we then detected whether SNHG11 influenced the interaction of the DICER-TRBP complex with pre-miR-1276 and pre-miR-483. The data for an RNA-binding protein IP (RIP) assay showed that inhibiting SNHG11 in MKN-45 and SGC-7901 cells increased the enrichment of pre-miR-1276 and pre-miR-483 in the precipitates induced by anti-TRBP and anti-DICER (Figure S10D). On the contrary, overexpressing SNHG11 reduced the enrichment of pre-miR-483 and pre-miR-1276 in the RIP products of antibodies against DICER and TRBP, while the overexpression of SNHG11 with mutated binding sites for pre-miR-483 or pre-miR-1276 failed to reduce the interaction of DICER and TRBP with pre-miR-483 or pre-miR-1276 in AGS cells (Figure S10E). Hence, we validated that SNHG11 not only acts as a ceRNA that interacts with mature miR-1276 and miR-483-3p to block their inhibitory effect on CTNNB1, but it also binds to pre-miR-1276 and pre-miR-483 to block their processing into mature miR-1276 and miR-483-3p.

miR-483-3p and miR-1276 Elicit Tumor-Suppressive Functions in GC

Then, we tested the functions of miR-483-3p and miR-1276 in GC. As a result, overexpression of miR-483-3p or miR-1276 alone reduced the proliferation of SGC-7901 and MKN-45 cells, and co-overexpression of miR-483-3p and miR-1276 further enhanced the reductive effect (Figure S11A and S11B). Also, both the sphere formation efficiency and $CD133^+$ ratio of GC cells were lowered under respective overexpression of miR-1276 or miR-483-3p, and co-overexpression of both miRNAs further strengthened such an effect (Figures S11C and S11D). Moreover, the migration and invasion of two GC cell lines were hindered under respective transfection of the miR-1276 mimic or miR-483-3p mimic, and the motilities were further restrained in response to the co-transfection of the miR-1265 mimic and miR-483-3p mimic (Figures S11E and S11F). Meanwhile, the capacities of GC cells to adhere to matrix were increased under respective upregulation of miR-1276 or miR-483-3p, and further enhanced after co-overexpressing both miRNAs (Figure S11G). Altogether, miR-483-3p and miR-1276 inhibited cell proliferation, stemness, migration, invasion, and matrix adhesion in GC.

SNHG11 Regulates the Wnt/β-Catenin Pathway and GC Progression Partly through miR-483-3p/miR-1276

Intriguingly, we found that either the respective inhibition or co-inhibition of miR-483-3p and miR-1276 could only partly reverse the induction of E-cadherin and the reduction of N-cadherin, MMP2, MMP7, Twist, Nanog, and OCT4 in SNHG11-silenced GC cells (Figure S12A). Neither respectively inhibiting miR-483-3p and miR-1276 nor jointly inhibiting them resulted in a full recovery of Wnt/β-catenin activity and nuclear expression of β-catenin in GC cells with SNHG11 knockdown (Figures S12B and S12C). Functionally, we verified that the suppressive impacts of deficient SNHG11 on GC cell proliferation, stemness, migration, and invasion were only partially counteracted by respective knockdown of miR-483-3p or miR-1276. Co-inhibition of miR-483-3p and miR-1276 further enhanced the recovery, but a full recovery was still not achieved (Figures S12D–S12G). In short, these data proved that SNHG11 regulates the Wnt/β-catenin pathway and the biological processes in GC partly through miR-483-3p/miR-1276.

SNHG11 Induces the Ubiquitination of GSK-3β by Interacting with CUL4A to Activate the Wnt/β-Catenin Pathway

Since we have found that regulating miR-483-3p/miR-1276 is not the only way for SNHG11 to affect the Wnt/β-catenin pathway, we continued to explore other manners in which SNHG11 regulates this pathway. It is known that GSK-3β is a key inhibitor of the Wnt/β-catenin pathway, which triggers the phosphorylation and degradation of β-catenin.[58] Therefore, we wondered whether SNHG11 might also regulate GSK-3β in GC. Results showed that the absence of SNHG11 induced the protein level of GSK-3β rather than the mRNA level of GSK-3β (Figure S13A), indicating that

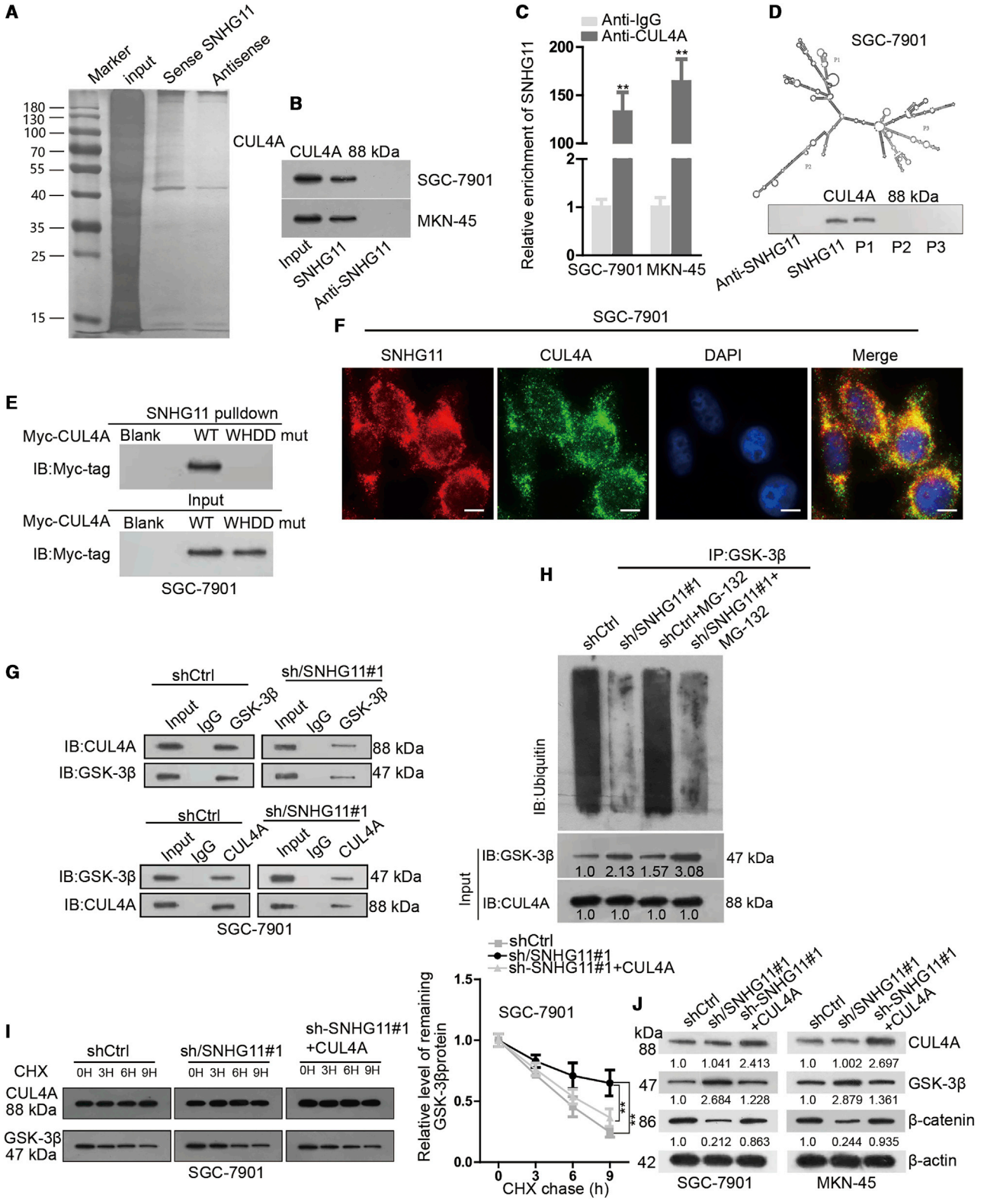

(legend on next page)

SNHG11 regulated GSK-3β at the protein level. To find out how SNHG11 regulates GSK-3β, we conducted an RNA pull-down assay and then mass spectrometry analysis of the proteins potentially interacting with SNHG11. Results indicated that CUL4A interacted with SNHG11 in both of the GC cell lines (Figures 5A and 5B). CUL4A is a ubiquitin ligase predominantly expressed in cytoplasm, and it has been reported to drive cancer progression through inducing the ubiquitination of several tumor-suppressive proteins such as LATS1, p21, and p53.[59] Therefore, we speculated that SNHG11 might regulate GSK-3β through CUL4A. To testify this speculation, we carried out a series of experiments. The results of RIP analysis evidenced the abundant existence of SNHG11 in the immunoprecipitated products of anti-CUL4A (Figure 5C). Then, to determine the precise interacting part, we predicted the secondary structure of SNHG11 and design oligonucleotide probes accordingly. We observed that CUL4A protein was specifically captured by WT SNHG11 and P1, indicating that P1 was required for the interaction of SNHG11 with CUL4A (Figure 5D). Furthermore, the winged helix-turn-helix DNA-binding domain (WHDD) domain of CUL4A has been reported to be crucial for the binding of CUL4A to DNA or RNA.[60] Hence, we tried to detect whether the WHDD domain is responsible for the interaction of CUL4A with SNHG11. As expected, the Myc-tagged WT CUL4A was enriched whereas the Myc-tagged CUL4A with the WHDD domain mutation was undetectable in the pull-down of the SNHG11 WT (Figure 5E). Also, the results of FISH and IF staining unveiled the co-localization of SNHG11 and CUL4A in the cytoplasm of GC cells (Figure 5F). Later on, a coimmunoprecipitation (coIP) assay showed that CUL4A was enriched in the immunoprecipitated products of GSK-3β and vice versa, indicating the interaction between CUL4A and GSK-3β. Also, when knocking down SNHG11, the interaction between GSK-3β and CUL4A was decreased, with the GSK-3β level in input increased and the CUL4A level unchanged (Figure 5G). We further validated that the ubiquitination level of GSK-3β was reduced in response to the knockdown of either SNHG11 or CUL4A. The addition of MG132, the proteasome inhibitor, further enhanced the inductive effect of sh/SNHG11#1 on the level of GSK-3β (Figures 5H and S13B). Of note, after the addition of cycloheximide (CHX) to inhibit protein generation, we observed through western blot that the degradation of GSK-3β was retarded under the knockdown of SNHG11, but such a retarding effect was offset in the face of upregulation of CUL4A (Figure 5I). Moreover, the knockdown of SNHG11 induced the GSK-3β level and reduced the β-catenin level without affecting CUL4A, and the co-transfection of pcDNA3.1/CUL4A increased the CUL4A level and reversed the alteration of GSK-3β and β-catenin levels (Figure 5J). In sum, SNHG11 induced the ubiquitination of GSK-3β by interacting with CUL4A to activate the Wnt/β-catenin pathway.

SNHG11 Induces Autophagy and Activates the Wnt/β-Catenin Pathway to Promote GC Progression

To assess whether SNHG11 regulates the Wnt/β-catenin pathway and GC progression through miR-483-3p/miR-1276 and GSK-3β, we designed and conducted corresponding rescue assays. Similarly, respective inhibition of miR-483-3p/miR-1276 or GSK-3β partly counteracted the suppressive effect of silenced SNHG11 on Wnt/β-catenin activity and nuclear expression of β-catenin, and a full counteraction was achieved by the joint inhibition of miR-483-3p/miR-1276 and GSK-3β (Figures S14A and S14B). These data suggested that SNHG11 activated Wnt/β-catenin through miR-483-3p/miR-1276 and GSK-3β. However, western blot analysis revealed that either respective or joint inhibition of miR-483-3p/miR-1276 or GSK-3β only partially counteracted the effect of SNHG11 on the levels of N-cadherin, N-cadherin, MMP2, MMP7, Twist, Nanog, and OCT4 (Figure S14C), indicating that SNHG11 regulated EMT and stemness of GC cells partly depending on the Wnt/β-catenin pathway. Because we showed that autophagy aggravated GC cell progression, Rapa was applied in subsequent rescue assays. As anticipated, we found that the repressive influences of SNHG11 depletion on cell viability, stemness, migration, and invasion were only partly restored after jointly inhibiting miR-483-3p/miR-1276 and GSK-3β, but inhibiting miR-483-3p/miR-1276 and GSK-3β jointly with Rapa treatment led to a full restoration of these processes (Figures S14D–S14G). These findings suggested that SNHG11 accelerates the malignant behaviors of GC cells depending on its modulation on autophagy and the Wnt/β-catenin pathway.

SNHG11 Is Transcriptionally Induced by TCF7L2 in GC Cells

Thereafter, we tried to explain the upregulation of SNHG11 in GC cells. Transcription factors are commonly considered to be responsible for the dysregulation of certain genes in cancer cells. Intriguingly, we found through the UCSC genome browser (http://genome.ucsc.edu/) that the promoter of SNHG11 harbors potential TCF7L2 binding sites (Figure S15A). As is widely known, TCF7L2 forms a transcriptional complex with β-catenin to activate downstream factors.[61] In this way, TCF7L2 exerts vital effects on cellular

Figure 5. SNHG11 Interacts with CUL4A to Induce the Ubiquitination of GSK-3β

(A) Proteins interacting with SNHG11 were identified through a pull-down assay and mass spectrometry analysis in GC cells. (B) Western blot analysis of pull-down products in GC cells confirmed the interaction between CUL4A and SNHG11. (C) Quantitative real-time RT-PCR analysis of RIP products validated the interaction of SNHG11 with CUL4A. (D) Secondary structure of SNHG11 was predicted through a bioinformatics tool (http://rna.tbi.univie.ac.at//cgi-bin/RNAWebSuite/RNAalifold.cgi). The pull-down assay plus western blot detected CUL4A in the pull-down products of indicated biotinylated RNAs. (E) Pull-down experiments and western blot detected Myc-tagged CUL4A (with wild-type or mutated WHDD domain) in the pull-down products of biotinylated SNHG11 in GC cells. (F) FISH and IF staining confirmed the co-localization of SNHG11 and CUL4A in GC cells. Scale bars, 20 μm. (G) coIP followed by western blot detected CUL4A and GSK-3β in the products precipitated by anti-GSK-3β or anti-CUL4A versus anti-IgG in GC cells transfected with shCtrl or sh/SNHG11#1. (H) Ubiquitination of GSK-3β in GC cells transfected with shCtrl or sh/SNHG11#1 and treated with or without MG-132, as well as GSK-3β level in inputs, was determined by western blot. (I) Level of CUL4A in GC cells of indicated groups was determined at the indicated time points, and the corresponding quantification curve was exhibited. (J) Western blots of CUL4A, GSK-3β, and β-catenin in GC cells of each group. Error bar denotes SD. $^{**}p < 0.01$.

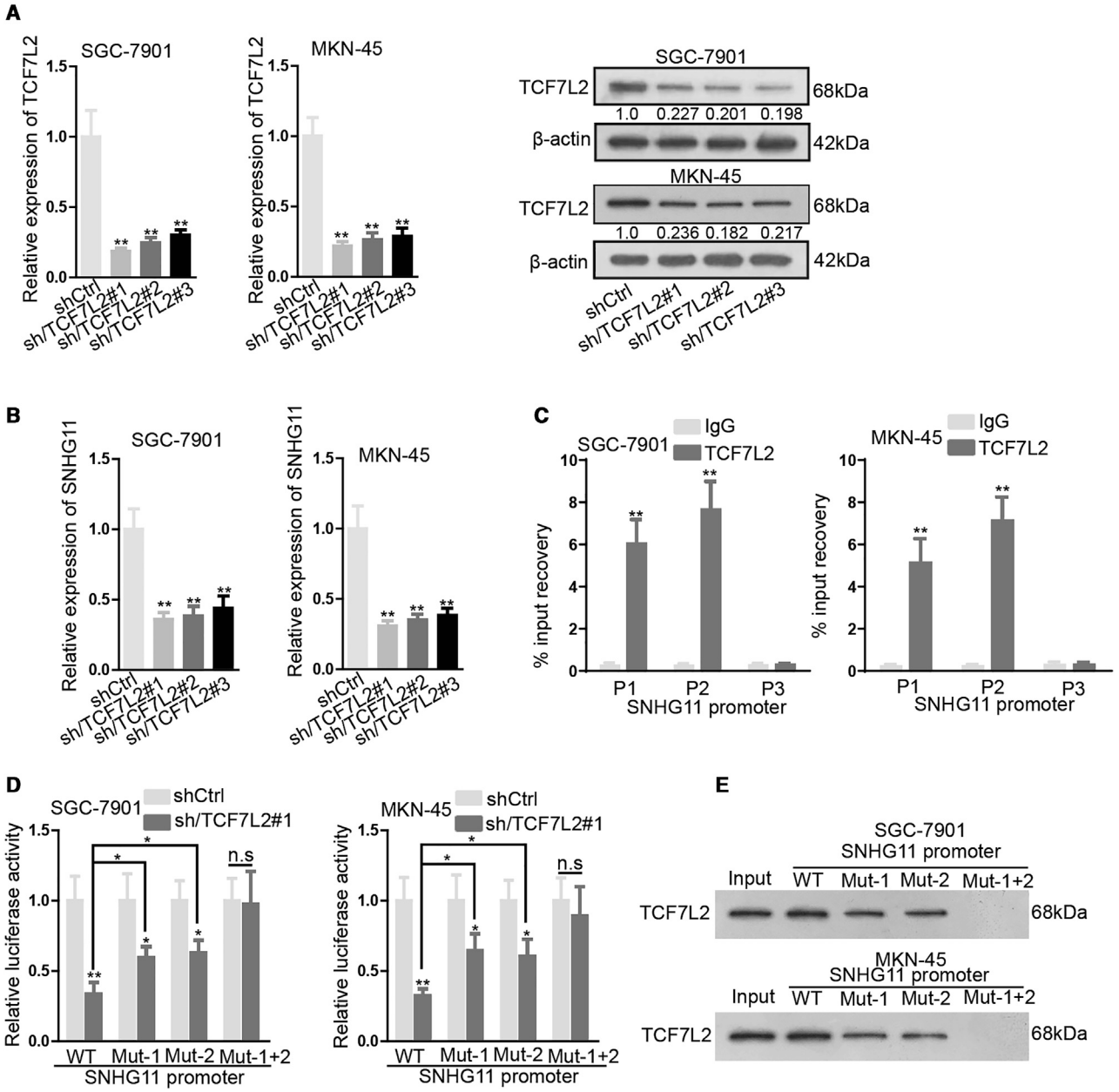

Figure 6. SNHG11/Wnt/β-Catenin Forms a Positive Feedback Loop

(A) Knockdown of TCF7L2 in GC cells by three shRNAs was determined by quantitative real-time RT-PCR and western blot. (B) Expression of SNHG11 in GC cells under TCF7L2 knockdown was determined by quantitative real-time RT-PCR. (C–E) ChIP analysis, a luciferase reporter assay, and a pull-down assay determined the relationship between TCF7L2 and the SNHG11 promoter. Error bar denotes SD. *p < 0.05, **p < 0.01. n.s., not significant.

behaviors such as cell proliferation, cell death, stress response, metabolism, and differentiation.[62] Hence, we wondered whether SNHG11 could be regulated at the transcriptional level by the TCF7L2/β-catenin complex. We knocked down TCF7L2 using three shRNAs and confirmed the overt reduction of TCF7L2 mRNA and protein expressions in SGC-7901 and MKN-45 cells (Figure 6A). The knockdown of TCF7L2 reduced the SNHG11 level in GC cells (Figure 6B). To investigate the detailed relationship between TCF7L2 and SNHG11, we identified two potential TCF7L2 binding sites on the SNHG11 promoter through JASPAR (Figure S15B). In the meantime, primers were designed for two parts of SNHG11 promoter fragments respectively containing the predicted binding sites 1 and 2 (P1 and P2), and for a region that does not contain predicted TCF7L2 sites (P3) (Figure S15B). As a result, we discovered that P1 and P2, instead of P3,

of the SNHG11 promoter were enriched in the precipitates of TCF7L2 (Figure 6C), indicating that TCF7L2 binds to the SNHG11 promoter at both sites 1 and 2. Moreover, we illustrated that silencing TCF7L2 attenuates the luciferase activity of SNHG11 promoter, which was partly recovered by the respective mutation of site 1 or 2 on the SNHG11 promoter; however, TCF7L2 knockdown could not alter the luciferase activity of reporters covering both site-mutated SNHG11 promoter sequences (Figure 6D). The pull-down assay illustrated that TCF7L2 was enriched in the pull-down by the WT SNHG11 biotin probe, and such enrichment was lessened in the pull-down of SNHG11 with site 1 or site 2 mutation, whereas no TCF7L2 was captured by SNHG11 with the mutation of both sites (Figure 6E). Taken together, the aforementioned data suggested that SNHG11 is transcriptionally activated by TCF7L2 in GC cells, which means that SNHG11/Wnt/β-catenin forms a positive feedback loop in GC.

SNHG11 Induces Autophagy and Activates the Wnt/β-Catenin Pathway to Promote GC Tumorigenesis *In Vivo*

In vivo assays were further carried out to examine whether the Wnt/β-catenin pathway and autophagy mediate the impact of SNHG11 on tumorigenesis and metastasis in GC. The tumor growth rate and tumor weight of xenografts were decreased by sh/SNHG11#1, and the effect of sh/SNHG11#1 was partially countervailed by anti-miR-483-3p+anti-miR-1276+small interfering RNA (siRNA) (si-)GSK-3β, and further addition of Rapa achieved a full reversion (Figures 7A and 7B). Meanwhile, the lowered positivity of Ki67 and CD133 in xenografts with SNHG11 knockdown was partly restored by the co-inhibition of miR-483-3p/miR-1276 plus GSK-3β, and was fully reversed with additional treatment of Rapa (Figures 7C and S15C). Also, western blot data confirmed that the induction of E-cadherin and the reduction of N-cadherin, MMP7, and MMP2, as well as the decline of stemness markers, in xenografts with SNHG11 inhibition were partly reversed by anti-miR-483-3p +anti-miR-1276+si-GSK-3β, but were fully recovered after additional Rapa treatment (Figure 7D). Also, the number of metastatic nodes reduced by sh/SNHG11#1 *in vivo* were partly recovered by co-inhibition of miR-483-3p/miR-1276 and GSK-3β, and further addition of Rapa led to a full recovery (Figure 7E). Interestingly, we also found that co-inhibiting miR-483-3p, miR-1276, and GSK-3β partly reversed the reduction of LC3-I/LC3-II rate and LAMP1 level, and the induction of p62 caused by SNHG11 knockdown in xenografts and a full reverse were observed when further adding Rapa (Figure 7F). Since we had previously demonstrated that Wnt/β-catenin cannot mediate the activating effect of SNHG11 on autophagy in GC cells, we deduced that it is miR-483-3p and miR-1276 that cause the recovery. Altogether, it was suggested that SNHG11 induces autophagy and activates Wnt/β-catenin pathway to promote GC tumorigenesis and metastasis *in vivo*.

SNHG11 Upregulates ATG12 through miR-483-3p/miR-1276 to Induce Autophagy

Finally, we tried to investigate whether SNHG11 regulates autophagy in GC through miR-483-3p and miR-1276. We found that the inhibition of either miR-483-3p or miR-1276 partially reversed the reduced LC3-II/LC3-I ratio and LAMP1 level and the elevated p62 level caused by sh/SNHG11#1 in GC cells, and such reversion was further strengthened by the co-inhibition of both miRNAs (Figure 8A and S16A), indicating that both miR-483-3p and miR-1276 were implicated in the facilitation of SNHG11 on autophagy in GC cells. We then browsed starBase3.0 and found that MAP1LC3B, GABARAPL1, and ATG12 are target genes shared by miR-483-3p and miR-1276, and these three factors are central participants in autophagy, as reported in previous studies.[47,63] However, the outcomes of a luciferase reporter assay showed that only the luciferase activity of the pmirGLO-ATG12 3′ UTR reporter was reduced by both miR-483-3p and miR-1276 mimics in two GC cell lines (Figures 8B and S16B). ATG12 is referred to as the "core" of autophagy machinery, which participates in autophagy by forming a complex with ATG5-ATG16 to decorate and expand phagophores.[64,65] Also, ATG12 has been reported to positively regulate oncogenic autophagy in GC.[66] miR-1276 also presents an inhibitory effect on the luciferase activity of MAP1LC3B, indicating the interaction between miR-1276 and MAP1LC3B. It is known that MAP1LC3B encodes LC3, and the transformation from one isoform LC3-I to another isoform LC3-II is an important indicator of autophagy activation.[67] Nonetheless, it has also been reported that artificially tethering LC3 to organelles is not sufficient to trigger autophagy,[68] indicating that the increase of LC3 alone by regulating miR-1276 might be insufficient to explain the alteration of autophagy. Therefore, we only focused on the exploration on ATG12 in the present study. We verified that ATG12 was upregulated in GC specimens and cells (Figure S16C). Also, in GC tissues, the ATG12 level was negatively associated with miR-483-3p and miR-1276 levels, whereas it was positively related to SNHG11 expression (Figure S16D). Additionally, RIP analysis data illustrated that ATG12, SNHG11, miR-1276, and miR-483-3p were all enriched in the immunoprecipitated products of anti-Ago2 (Figures 8C and S16E). The binding sequences on the ATG12 3′ UTR for miR-483-3p and miR-1276 are presented in Figure 8D. Our results showed that co-overexpression of miR-483-3p and miR-1276 reduced the luciferase activity of the WT ATG12 3′ UTR reporter, and the reduction was more significant than that induced by overexpression of either the two miRNAs; moreover, such and effect was countervailed by the overexpression of SNHG11, with the luciferase activity of reporters with the mutant ATG12 3′ UTR (both sites mutated) having been unchanged all along (Figure 8E). Also, co-inhibition of miR-483-3p/miR-1276 counteracted the suppression of SNHG11 deficiency on ATG12 mRNA and protein levels, while the rescuing effect was more evident than the respective knockdown of miR-483-3p or miR-1276 (Figures 8F and S16F). Importantly, inhibiting miR-483-3p/miR-1276 restored SNHG11 suppression-inhibited autophagy in GC cells, while such restoration was abrogated in response to ATG12 silence (Figures 8G, 8I, and S16G). In conclusion, these data convincingly demonstrated that SNHG11 upregulates ATG12 through miR-483-3p/miR-1276 to induce autophagy.

DISCUSSION

lncRNAs have been suggested as promising diagnostic biomarkers and therapeutic targets in various types of cancers,[69] including

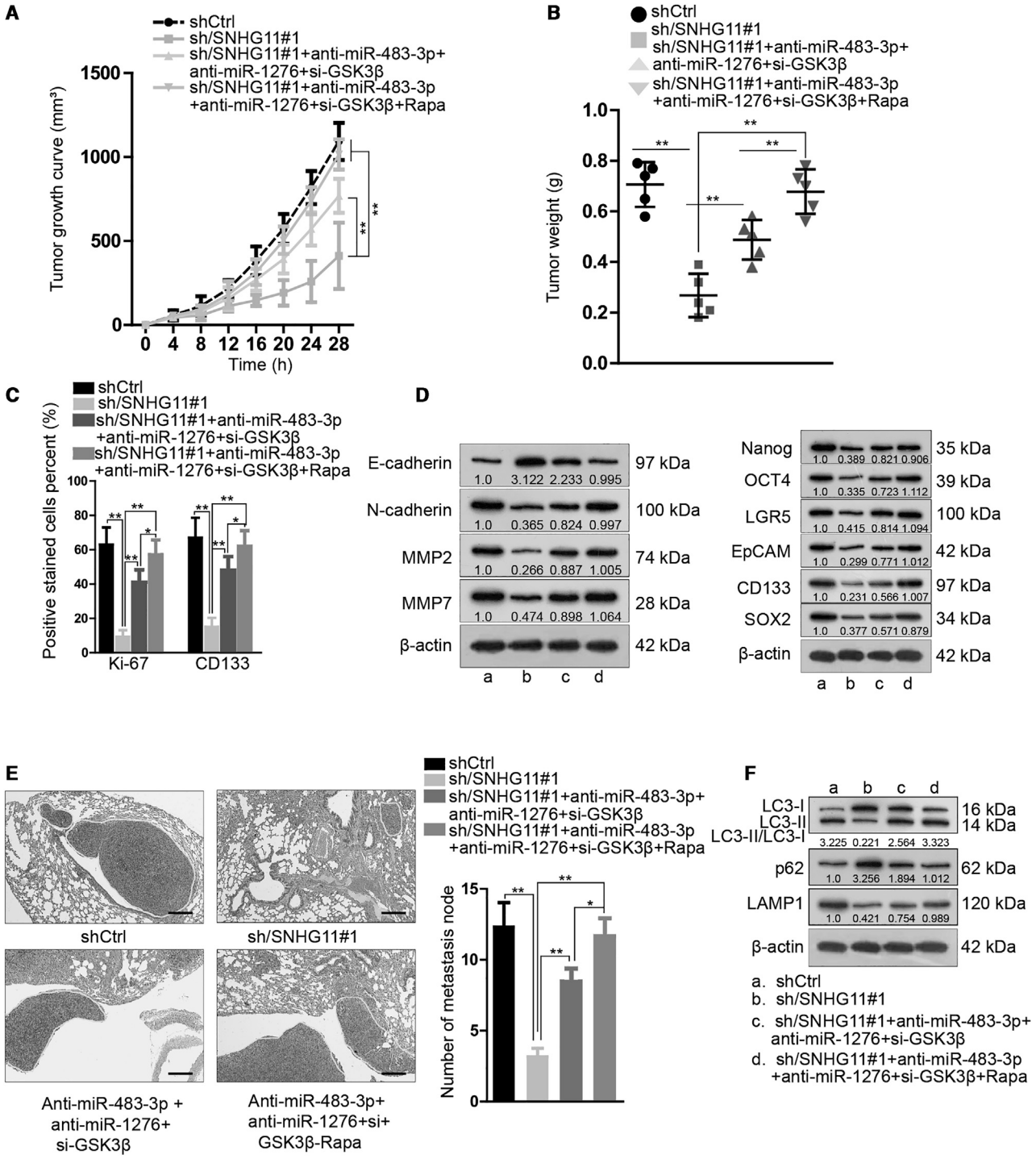

Figure 7. SNHG11 Promotes GC Progression through Wnt/β-Catenin and Autophagy *In Vivo*

(A and B) Growth curve (A) and tumor weight (B) of xenografts from mice in indicated groups. (C) The quantification of Ki67 and CD133 positivity determined by IHC staining in xenografts of each group. (D) Western blot results of EMT markers and stemness markers in xenografts of each group. (E) H&E staining of lung metastatic nodes and the quantification in mice from indicated groups. Scale bars, 200 μm. (F) Western blot results of autophagy-related proteins in xenografts of each group. Error bar denotes SD. *$p < 0.05$, **$p < 0.01$. n.s., not significant.

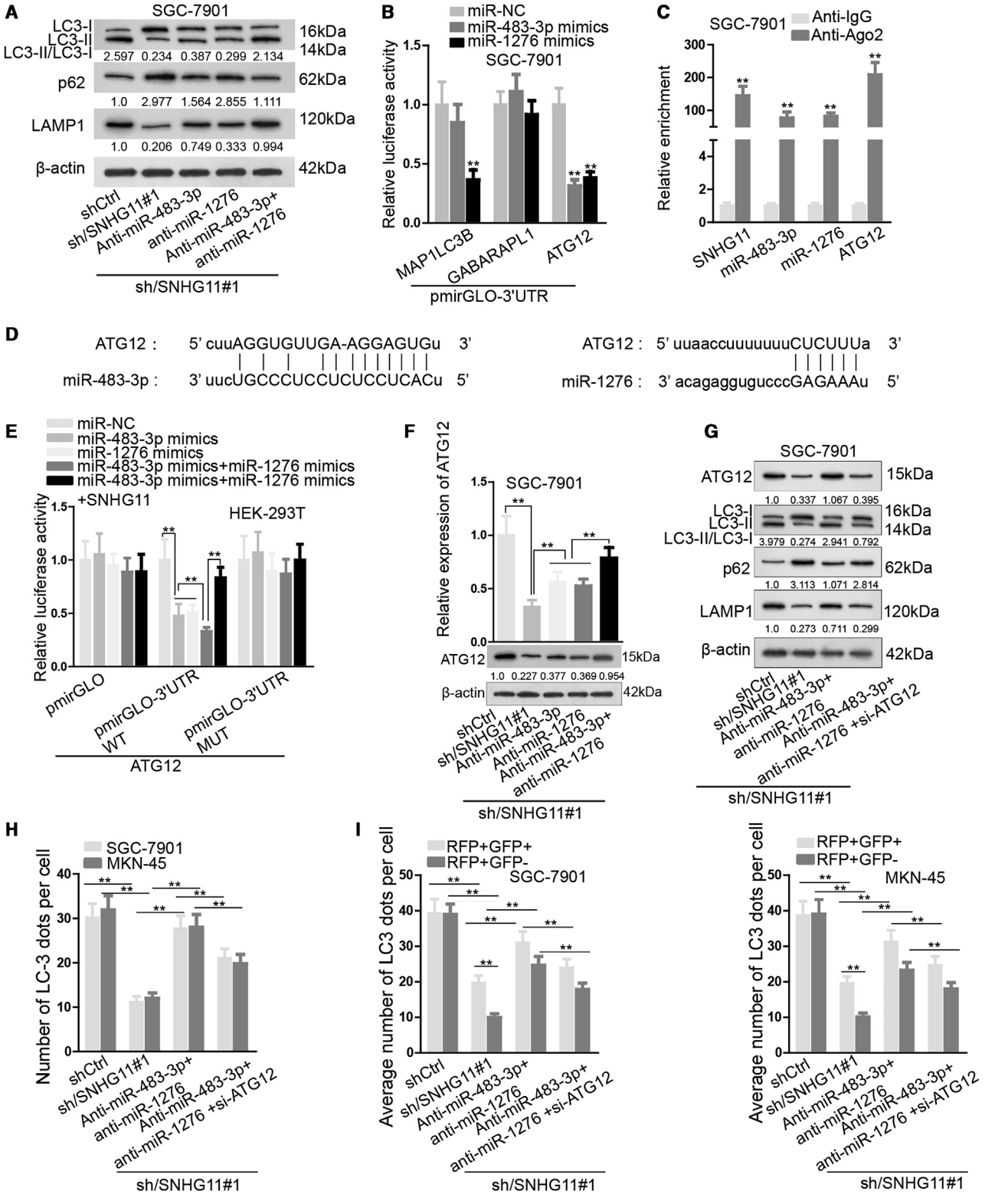

(legend on next page)

GC.[13,14] In the present study, we discovered that SNHG11 was upregulated in GC cell lines and specimens from GC patients. Furthermore, we suggested that SNHG11 upregulation predicted unfavorable survival outcomes and was related to advanced clinical stage and distant metastasis in GC patients. These data suggested that SNHG11 potentially participated in the tumor progression and metastasis in GC. As expected, we demonstrated that SNHG11 positively regulated *in vitro* cell proliferation and stemness, and *in vivo* tumorigenesis in GC. Additionally, SNHG11 also attenuated matrix adhesion and promoted GC cell migration, invasion, EMT, and anoikis resistance, as well as *in vivo* metastasis. These findings showed that SNHG11 played a positive regulatory role in tumorigenesis and metastasis of GC.

Moreover, we discovered that SNHG11 functioned as a positive regulator of autophagy in GC. Other studies have suggested that the effect of autophagy is controversial, because it either contributes to cell survival or to cell death depending on the cellular context.[70] Interestingly, Mowers et al.[29] pointed out that autophagy not only facilitates cell viability and differentiation, but it also regulates tumor metastasis through influencing anoikis resistance, migration, invasion, and EMT progression in tumor cells. Also, the oncogenic function of aberrant autophagy in GC has been recognized in several studies.[30,31] Accordingly, our data showed that the autophagic level in GC cells was higher than that in normal gastric cells, and inhibiting autophagy circumscribed the proliferation and metastasis of GC cells under starvation, indicating the oncogenic role of excessive autophagy in GC cells. Importantly, we first demonstrated that SNHG11 knockdown impaired autophagy in GC, indicating that SNHG11 regulated GC progression through inducing autophagy.

Wnt/β-catenin signaling is a well-known pathway participating in the regulation of cell survival, stemness, metastasis, and apoptosis in numerous cancer types,[32–34] including GC.[37,38] This study first found that SNHG11 positively regulated the Wnt/β-catenin pathway in GC cells. Intriguingly, Wnt/β-catenin mediated the contribution of SNHG11 to cell proliferation and metastasis, but it was not implicated in SNHG11-modulated autophagy in GC. The relationship between Wnt/β-catenin and autophagy is complicated and controversial. Some reports have illustrated that activation of Wnt/β-catenin leads to increased autophagy,[71] whereas others have argued that Wnt/β-catenin exhibits a suppressive effect on autophagy.[72,73] Previous studies have raised interesting findings that β-catenin induces p62 expression and inhibits autophagic flux in cancer cells under either stress or normal conditions.[73] Therefore, it was possible that activating Wnt/β-catenin could induce GC cell progression but inhibit autophagy. Considering that SNHG11 knockdown resulted in impaired autophagy in GC cells, it was possible that the activation of Wnt/β-catenin failed to have further suppressive effects on autophagy in such cells. Also, it is justified to suggest that the activation of SNHG11 on autophagy was independent of the Wnt/β-catenin pathway.

Mechanistically, we validated the cytoplasmic localization of SNHG11 in GC cells. In recent years, cytoplasmic lncRNAs have been disclosed to regulate target genes through various manners such as sponging miRNAs or interacting with RNA-binding proteins.[12] Herein, we first demonstrated that SNHG11 worked in GC through multiple mechanisms. As for the regulation of SNHG11 on Wnt/β-catenin, we first elucidated that SNHG11 sponged miR-483-3p and miR-1267 to protect CTNNB1 from the downregulation of miRNAs. Intriguingly, we also discovered that SNHG11 negatively regulated the expressions of miR-483-3p and miR-1267 by affecting the processing of their pre-miRNAs, as is a reported manner whereby cytoplasmic lncRNAs regulate miRNA expression.[55] Herein, we also first demonstrated that SNHG11 not only acted as a sponge of mature miR-483-3p and miR-1276, but it also bound to the loop residue of pre-miR-483 and pre-miR-1276 to block the DICER-TRBP-mediated splicing of pre-miRNA, reducing the expression of mature miR-483-3p and miR-1276. Furthermore, the partial recovery of Wnt/β-catenin activity by miR-483-3p and miR-1267 co-inhibition indicated that SNHG11 also regulated this pathway in other manners. Considering that the accumulation of cytoplasmic β-catenin could be impaired by GSK-3β-mediated phosphorylation,[58] we deduced that SNHG11 negatively regulated GSK-3β. We first demonstrated that SNHG11 induced the ubiquitination of GSK-3β by interacting with CUL4A, a cytoplasmic ubiquitin ligase contributing to cancer progression.[59] A former study indicated that CUL4A can be inhibited by lncRNA uc.134 to repress HCC progression,[60] while the relationship between CUL4A and SNHG11 was first revealed by our study. Moreover, we discovered that TCF7L2 bound to the SNHG11 promoter and induced the transactivation of SNHG11, indicating that SNHG11/Wnt/β-catenin formed a positive feedback loop in GC. Additionally, we found that SNHG11 could regulate autophagy through miR-483-3p/miR-1276-targeted ATG12, a pivotal regulator of autophagy, by forming a complex with ATG5-ATG16.[64,65] However, the partial rescue of autophagy by ATG12 in GC cells with SNHG11 knockdown indicated that SNHG11 might regulate autophagy through alternate targets, which remain to be further identified.

Figure 8. SNHG11 Induces Autophagy through miR-483-3p/miR-1276/ATG12 Axis

(A) Western blot results showed the level of autophagy-related proteins in GC cells under different transfections. (B) A luciferase reporter assay was used to determine the interaction of miR-483-3p and miR-1276 with three mRNAs (MAP1LC3B, GABARAPL1, and AGT12). (C) A RIP assay confirmed the interaction of miR-483-3p and miR-1276 with ATG12 and SNHG11. (D) Interacting sequences on ATG12 for miR-483-3p and miR-1276 were predicted through starBase 3.0. (E) A luciferase reporter assay indicated that SNHG11 regulated ATG12 through miR-483-3p and miR-1276. (F) Quantitative real-time RT-PCR and western blot results of ATG12 expression in GC cells of each group. (G) Western blot results of ATG12 and several autophagy-related proteins (LC3-II/LC3-I, p62, and LAMP1) in GC cells with indicated transfections. (H and I) Quantification of endogenous LC3 dots and exogenous GFP-mRFP-LC3 dots in GC cells with indicated transfections. Error bar denotes SD. $^{**}p < 0.01$.

MATERIALS AND METHODS

Tissue Specimens

50 GC specimens and the matched 50 para-tumorous specimens were included in this study. The histologic diagnosis of these clinical tissues was confirmed by three pathologists. Patients involved in the study received surgery at Tongren Hospital, Shanghai Jiao Tong University School of Medicine, and the fresh tissues were snap-frozen in liquid nitrogen and maintained at −80°C for subsequent studies. Written informed consent was obtained from all patients, and the study was approved by the Ethics Committee of Tongren Hospital, Shanghai Jiao Tong University School of Medicine.

Cell Lines and Cell Culture

The normal human gastric epithelial cell line GES-1 and six types of GC cell lines (SGC7901, BGC823, MGC-803, MKN45, HGC27, and AGS) were used in this study. These cell lines were all purchased from the Cell Bank of the Chinese Academy of Sciences (Shanghai, China). All cells were maintained in RPMI 1640 (Gibco, El Paso, TX, USA) with 10% fetal bovine serum (FBS, Gibco). Human embryonic kidney (HEK) 293T cells were obtained from the American Type Culture Collection (ATCC, Manassas, VA, USA) and maintained in DMEM (Gibco) with 10% FBS. Cell culture was carried out in a humidified incubator under 37°C with 5% CO_2.

lncRNA PCR Array

To find out the differentially expressed lncRNAs in GC cells versus normal GES-1 cells, a lncRNA PCR array was applied. The total RNAs extracted from GES-1, SGC-7901, and MKN-45 cells were subjected to reverse transcription by the rtStar first-strand cDNA synthesis kit (AS-FS-001, Arraystar) to obtain cDNA. Then, the cDNA and RNA were mixed with Arraystar SYBR Green quantitative real-time PCR master mix (AS-MR-005, Arraystar) and underwent quantitative real-time PCR to analyze the levels of 38 lncRNAs reported previously.[74]

Cell Transfection

To knock down SNHG11, CUL4A, or TCF7L2, the pLKO.1 constructs with sh/SNHG11#1/2/3, sh/CUL4A, or sh/TCF7L2#1/2/3 were applied. To knock down GSK-3β, si-GSK-3β was applied. Scrambled shRNAs (shCtrl) or siRNAs (si-Ctrl) were used as the negative controls. The sequences of shRNAs are provided in Table S1. To overexpress SNHG11 or CUL4A, pcDNA3.1 vectors inserted with a full-length cDNA sequence of SNHG11 or CUL4A were applied, and the recombinant plasmids were named as pcDNA3.1/SNHG11 or pcDNA3.1/CUL4A. The empty pcDNA3.1 vector was used as the negative control. To overexpress miR-483-3p and miR-1276, miR-483-3p mimics and miR-1276 mimics were applied, with miR-negative control (miR-NC) as the control. To inhibit miR-483-3p and miR-1276, anti-miRNA oligonucleotides (anti-miR-483-3p and anti-miR-1276) were applied, with anti-miR-NC as the negative control. Plasmids above were bought from Shanghai GenePharma (Shanghai, China) and transfected into SGC-7901 or MKN-45 cells as required by use of Lipofectamine 3000 (Thermo Fisher Scientific, Waltham, MA, USA).

Quantitative Real-Time RT-PCR

Total RNAs were extracted from GC specimens and indicated GC cells applying TRIzol reagent (Invitrogen), followed by reverse transcription using EvoScript Universal cDNA Master (Roche). Quantitative real time RT-PCR was conducted to examine the relative RNA level based on the SYBR Green method on the Roche LightCycler 480 PCR system, with β-actin as the endogenous control. The reverse transcription of miRNAs was conducted by a TaqMan miRNA reverse transcription kit (Applied Biosystems, Foster City, CA, USA). Quantitation of miRNAs was carried out by applying TaqMan miRNA assays (Applied Biosystems), with U6 small nuclear RNA as the internal control. Data were calculated based on $2^{-\Delta\Delta Ct}$ method. Primer sequences are provided in Table S2.

Western Blot

Total proteins were isolated from GC tissues and cells using radioimmunoprecipitation assay (RIPA) lysis buffer (Beyotime, Shanghai, China), loaded on and separated by the 10% SDS-PAGE (Bio-Rad, Hercules, CA, USA), and then transferred to the polyvinylidene fluoride (PVDF) membranes (Millipore, Bedford, MA, USA). Membranes were sealed in 5% nonfat milk, probed by primary antibodies overnight, and then incubated with secondary antibody for 1 h. An enhanced chemiluminescence (ECL) reagent (Pierce, Rockford, IL, USA) was used to visualize the immunoblots.

Antibodies and Reagents

Rabbit anti-Bcl2 (WL01556), rabbit anti-cleaved caspase-3 (WL01992), rabbit anti-cleaved PARP (WL01932), rabbit anti-BECN1 (WL02237), rabbit anti-β-catenin (WL0962a), rabbit anti-BAX (WL01637), and rabbit anti-ITGB1 (WL02236) were bought from Wanlei Biotechnology (Shanghai, China). Rabbit anti-p62 (A0682), rabbit anti-LC3II (A7198), and rabbit anti-p-AKT1-S473 (AP0140) were bought from ABclonal (Woburn, MA, USA). Rabbit anti-β-actin (ab8227), rabbit anti-Nanog (ab109250), mouse anti-Oct4 (ab184665), rabbit anti-SOX2 (ab137385), mouse anti-Twist (ab175430), goat anti-LGR5 (ab75850), rabbit anti-EpCAM (ab71916), rabbit anti-CD133 (ab19898), rabbit anti-LAMP1 (ab24170), rabbit anti-Gli1 (ab49314), rabbit anti-GLI2 (ab26056), rabbit anti-GLI3 (ab123495), anti-rabbit MMP2 (ab37150), rabbit anti-MMP7 (ab5706), mouse anti-E-cadherin (ab1416), rabbit anti-N-cadherin (ab18203), rabbit anti-CUL4A (ab72548), rabbit anti-ATG12 (ab155589), rabbit anti-cleaved caspase-6 (ab2326), rabbit anti-Ki67 (ab833), mouse anti-DICER (ab14601), and rabbit anti-TRBP (ab18094) were purchased from Abcam (Cambridge, UK). Rabbit anti-p-PI3K (Tyr458) (#4228), rabbit p-MAPK (Thr180/Tyr182) (#4511), rabbit p-STAT3 (Tyr705) (#9145), mouse anti-GSK-3β (#9832), mouse anti-Myc-tag (#2276), rabbit anti-ALDH1 (#36671), and rabbit anti-TCF7L2 (#2569) were purchased from Cell Signaling Technology (Danvers, MA, USA). Rapa (S1039) was purchased from Selleck Chemicals (Shanghai, China), while BafA1 (B1793) was purchased from Sigma-Aldrich (St. Louis, MO, USA).

Cell Proliferation Assay

Cell proliferation was evaluated through Cell Counting Kit-8 (CCK-8), colony formation, and EdU experiments as described previously.[75] The viability of SGC-7901 and MKN-45 cells was detected by a CCK-8 assay (Dojindo). The absorbance value was examined at 450 nm by applying the ELx800 microplate reader (BioTek, USA). For the colony formation assay, GC cells (5×10^2/well) were seeded in six-well plates, cultured for 2 weeks, and stained by crystal violet (Solarbio, G1062) after fixation. Colonies formed by >50 cells were counted manually. The colony formation efficiency was calculated as the number of colonies/number of seeded cells × 100%, and that of control groups was set as 1.0. For the EdU assay, an EdU labeling/detection kit (Ribobio, Guangzhou, China) was applied to stain the proliferative GC cells, and DAPI was used to stain cell nuclei. EdU-positive cells were observed through fluorescence microscopy, and the results were analyzed by the ratio of EdU-positive cell number versus DAPI-stained cell number.

Sphere Formation Assays

SGC-7901 and MKN-45 cells were plated into ultra-low attachment surface six-well culture plates (Corning Life Sciences, Corning, NY, USA) with the concentration of 3×10^3 cells/mL in DMEM/F12 medium (Gibco). The medium contained 20 ng/mL basic fibroblast growth factor (bFGF), 20 ng/mL epidermal growth factor (EGF), and 2% B27. Diameters of spheres were measured every 7 days after seeding. Images of five randomly chosen regions in each group were captured with a fluorescence microscope (Leica, Wetzlar, Germany). The sphere formation efficiency was calculated as the number of spheres/number of seeded cells × 100%, and that of control groups was set as 1.0.

Flow Cytometry Assay

The apoptosis of GC cells was analyzed via a fluorescence-activated cell sorting (FACS) flow cytometer (BD Biosciences, San Jose, CA, USA) after annexin V-fluorescein isothiocyanate (FITC)/propidium iodide (PI) staining. The procedure followed previous descriptions.[76]

For flow cytometry analysis of cell surface expression of $CD133^+$ in GC cells, CD133-phycoerythrin (PE) antibodies (Miltenyi Biotec, Auburn, CA, USA) were applied. In short, the harvested GC cells were washed twice and underwent re-suspension in Hanks' balanced salt solution (HBSS). After incubation with antibodies in darkness for 30 min at room temperature, cells were washed and detected by a flow cytometer (BD Biosciences) and analyzed on FlowJo software (BD Biosciences).

Transwell Migration and Invasion Assay

To evaluate cell invasion and migration, a transwell assay was conducted. GC cells were plated into the upper transwell chamber (8-μm pore size; Millipore) in non-serum media. The upper chamber of the insert was pre-coated with Matrigel (Sigma-Aldrich) for the invasion assay rather than for the migration assay. Medium in the lower chamber contained 10% FBS. Cells were cultured for 24 h, and those migrating or invading to the lower chamber were respectively fixed and stained using methanol and crystal violet, followed by imaging and counting under the inverted microscope (Olympus, Tokyo, Japan).

Cell Matrix Adhesion Assay

96-well plates were coated with FN1/fibronectin (10 mg/mL, Sigma, 10838039001) overnight at 4°C and blocked by 1% (w/v) BSA (Sigma, A7030). GC cells (5×10^4/well) seeded in the plates were allowed to adhere at 37°C for 10 min and underwent a PBS wash three times. Then, cells were fixed and stained using 4% paraformaldehyde (Sigma, V900894) and 0.5% crystal violet (Solarbio, G1062) and lysed using 30% (v/v) glacial acetic acid (Aladdin, A116172). An Olympus IX 71 was used to image the cells on the substrate 1.5 h later and then the results were analyzed by Image-Pro Plus software.

FISH and IF

FISH and IF staining assays were performed according to former descriptions.[77] For FISH staining, a QuantiGene ViewRNA miRNA ISH cell assay kit (Affymetrix, Santa Clara, CA, USA) was applied with the probe targeting SNHG11 in line with the manufacturer's guidance. For IF staining, antibodies against LC3 (SRP01707, Saier Biotechnology), E-cadherin (ab1416, Abcam), N-cadherin (ab18203, Abcam), ALDH1 (#36671, Cell Signaling Technology), and CUL4A (ab72548, Abcam) were applied. The samples were then observed under a fluorescence microscope (DMI4000B, Leica).

GFP-mRFP-LC3 Adenoviral Transfection

GC cells were plated on the glass-bottomed cell culture dishes and infected with GFP-mRFP-LC3 adenoviral vectors (HanBio Technology, Shanghai, China). After replacing the culture medium with fresh medium, GC cells were incubated for 1 d. The yellow and green dots were observed under a confocal laser scanning microscope (LSM 880 with Airyscan; Zeiss, Dublin, CA, USA) to determine autophagy flux.

TOP/FOP Flash Reporter Assays

A TOP/FOP flash reporter assay was applied to determine the activity of the Wnt/β-catenin pathway. The TOP-flash Wnt signaling reporter and FOP-flash negative control reporter were co-transfected with indicated plasmids into GC cells obeying the manufacturer's protocol (Millipore, 17-285). GC cells underwent transfection with pTOP-Flash (TCF reporter plasmid) or pFOP-Flash (mutant, inactive TCF binding site) plasmids, with the pSV40-Renilla plasmid (Promega, E6911) as the internal control. 48 h after transfection, the luciferase activities were analyzed by the Dual-Luciferase reporter assay system (Promega, e1910).

ChIP, RIP, and Pull-Down Assay

A chromatin IP (ChIP) assay was carried out using the MagnaChIP kit (Millipore) with antibodies against TCF7L2 (#2569, Cell Signaling Technology) referring to the manufacturer's guidance as described previously.[78] A RIP assay was conducted using a Magna RIP (Millipore, Bedford, MA, USA) following the manufacturer's instructions. Antibodies against Ago2 (ab32381, Abcam), immunoglobulin G (IgG) (ab190475, Abcam), and CUL4A (ab72548, Abcam) were

applied. The immunoprecipitated products were analyzed through quantitative real-time RT-PCR.

For the pull-down assay, the biotin-labeled RNA SNHG11 and antisense SNHG11 sequences were transcribed *in vitro* using biotin RNA labeling mix (Roche) and T7 RNA polymerase (Roche) following treatment with RNase-free DNase I (Roche) and 0.2 M EDTA to block the reaction. GC cells were transfected with pcDNA3.1(+)/CUL4A-Myc (WT) and pcDNA3.1(+)/CUL4A-Myc (WHDD mutant) with the WHDD domain of CUL4A mutated. After the biotinylated RNAs and streptavidin agarose beads (Life Technologies, Gaithersburg, MD, USA) were mixed for 12 h at 4°C, cell lysates and RNase inhibitor were added and incubated for another 4 h on ice. After the mixture was boiled in the SDS buffer, the proteins were detected by western blot. The SNHG11-interacting proteins were eluted and resolved via gel electrophoresis, and then subjected to staining via SilverQuest silver staining kit (LC6070, Thermo Fisher Scientific). The excised protein bands were de-stained and digested, followed by the analysis via liquid chromatography-tandem mass spectrometry sequencing (LCMS-8060, Shimadzu, Japan).

IP and Ubiquitination Assays

An IP assay was conducted applying the Thermo Scientific Pierce Classic IP kit (Thermo Fisher Scientific, MA, USA) in accordance with the manufacturer's instructions. GC cells with indicated transfections were treated with or without MG-132 (2 μM; the inhibitor of proteasome) for 48 h. Then, cells were lysed in the IP lysis/wash buffer with protease inhibitors and RNase inhibitor (Promega, Madison, WI., USA) followed by centrifugation. The protein A/G beads (Life Technologies) conjugated with antibodies against GSK-3β (#9832, Cell Signaling Technology) or CUL4A (ab72548, Abcam) were mixed with cell lysates for 12 h at 4°C with rotation, and boiled in the SDS buffer. Thereafter, the eluted proteins were analyzed by western blot.

Animal Experiments

Male BALB/c nude mice (age, 4–6 weeks) were purchased from the Medical Laboratory Animal Center (Guangdong, China). The experiments were approved by the Institutional Animal Care and Use Committee of Tongren Hospital, Shanghai Jiao Tong University School of Medicine. All mice were kept under a specific pathogen-free condition with free access to food and water. To establish xenografts, mice were injected subcutaneously with MKN-45 cells transfected with indicated plasmids. The size of tumors was measured every 4 days. After 28 days of injection, the tumors were resected for further assays. To monitor the impact of SNHG11 on GC metastasis, transfected MKN-45 cells were injected into mice via the tail vain. Six weeks later, mice were sacrificed and the metastatic nodes in lung or liver tissues were observed by H&E staining.

Immunohistochemistry (IHC) and H&E Staining

IHC staining of the xenografts from mice was conducted following a previous description.[79] The antibodies against Ki67 (ab833, Abcam) and CD133 (ab19898, Abcam) were applied. The metastatic nodules were observed by H&E staining as formerly described.[80]

Statistical Analysis

To analyze data, SPSS version 13.0 (SPSS, Chicago, IL, USA) software was applied. Data were expressed based on mean ± standard deviation (SD) unless otherwise indicated. Statistical methods for data analysis were one-way analysis of variance (ANOVA) or Student's t tests, as needed. All experiments were performed in triplicate. Statistical significance was determined by a p value <0.05.

SUPPLEMENTAL INFORMATION

Supplemental Information can be found online at https://doi.org/10.1016/j.ymthe.2020.10.011.

ACKNOWLEDGMENTS

Thank you to all who were involved in this study. This work was supported by The Research Fund of Shanghai Tongren Hospital, Shanghai Jiaotong University School of Medicine (nos. TRYJ201511 and TRYJ201613); the Shanghai Municipal Health Commission (20194Y0373); the National Natural Science Foundation of China (nos. 81570549 and 81472242); the Shanghai Municipal Health Bureau Key Disciplines Grant (no. ZK2015A24); the Natural Science Foundation of the Science and Technology Commission of Shanghai Municipality (nos. 15411971000 and 16411972700).

AUTHOR CONTRIBUTIONS

Q.W., J.M., and J.W. designed the whole work. Then, Q.W. and J.M. designed the experiments, J.W. and W.M. conducted the experiments, Q.W., Y.W., and M.S. collected and analyzed all the data, and all of the co-authors shared in writing the manuscript.

DECLARATION OF INTERESTS

The authors declare no competing interests.

REFERENCES

1. Ferlay, J., Shin, H.-R., Bray, F., Forman, D., Mathers, C., and Parkin, D.M. (2010). Estimates of worldwide burden of cancer in 2008: GLOBOCAN 2008. Int. J. Cancer *127*, 2893–2917.

2. Siegel, R., Naishadham, D., and Jemal, A. (2013). Cancer statistics, 2013. CA Cancer J. Clin. *63*, 11–30.

3. Dassen, A.E., Dikken, J.L., van de Velde, C.J.H., Wouters, M.W.J.M., Bosscha, K., and Lemmens, V.E.P.P. (2013). Changes in treatment patterns and their influence on long-term survival in patients with stages I–III gastric cancer in the Netherlands. Int. J. Cancer *133*, 1859–1866.

4. Catalano, V., Labianca, R., Beretta, G.D., Gatta, G., de Braud, F., and Van Cutsem, E. (2009). Gastric cancer. Crit. Rev. Oncol. Hematol. *71*, 127–164.

5. Deng, M., Zeng, C., Lu, X., He, X., Zhang, R., Qiu, Q., Zheng, G., Jia, X., Liu, H., and He, Z. (2017). miR-218 suppresses gastric cancer cell cycle progression through the CDK6/cyclin D1/E2F1 axis in a feedback loop. Cancer Lett. *403*, 175–185.

6. Flintoft, L. (2013). Non-coding RNA: structure and function for lncRNAs. Nat. Rev. Genet. *14*, 598.

7. Hung, T., Wang, Y., Lin, M.F., Koegel, A.K., Kotake, Y., Grant, G.D., Horlings, H.M., Shah, N., Umbricht, C., Wang, P., et al. (2011). Extensive and coordinated transcription of noncoding RNAs within cell-cycle promoters. Nat. Genet. *43*, 621–629.

8. Huarte, M., Guttman, M., Feldser, D., Garber, M., Koziol, M.J., Kenzelmann-Broz, D., Khalil, A.M., Zuk, O., Amit, I., Rabani, M., et al. (2010). A large intergenic noncoding RNA induced by p53 mediates global gene repression in the p53 response. Cell *142*, 409–419.

9. He, W., Liang, B., Wang, C., Li, S., Zhao, Y., Huang, Q., Liu, Z., Yao, Z., Wu, Q., Liao, W., et al. (2019). MSC-regulated lncRNA MACC1-AS1 promotes stemness and chemoresistance through fatty acid oxidation in gastric cancer. Oncogene *38*, 4637–4654.

10. Yue, B., Liu, C., Sun, H., Liu, M., Song, C., Cui, R., Qiu, S., and Zhong, M. (2018). A positive feed-forward loop between lncRNA-CYTOR and Wnt/β-catenin signaling promotes metastasis of colon cancer. Mol. Ther. *26*, 1287–1298.

11. YiRen, H., YingCong, Y., Sunwu, Y., Keqin, L., Xiaochun, T., Senrui, C., Ende, C., XiZhou, L., and Yanfan, C. (2017). Long noncoding RNA *MALAT1* regulates autophagy associated chemoresistance via miR-23b-3p sequestration in gastric cancer. Mol. Cancer *16*, 174.

12. Guttman, M., and Rinn, J.L. (2012). Modular regulatory principles of large non-coding RNAs. Nature *482*, 339–346.

13. Kong, F., Deng, X., Kong, X., Du, Y., Li, L., Zhu, H., Wang, Y., Xie, D., Guha, S., Li, Z., et al. (2018). ZFPM2-AS1, a novel lncRNA, attenuates the p53 pathway and promotes gastric carcinogenesis by stabilizing MIF. Oncogene *37*, 5982–5996.

14. Zhang, J.X., Chen, Z.H., Chen, D.L., Tian, X.P., Wang, C.Y., Zhou, Z.W., Gao, Y., Xu, Y., Chen, C., Zheng, Z.S., et al. (2018). LINC01410-miR-532-NCF2-NF-kB feedback loop promotes gastric cancer angiogenesis and metastasis. Oncogene *37*, 2660–2675.

15. Ye, G., Guo, L., Xing, Y., Sun, W., and Yuan, M. (2019). Identification of prognostic biomarkers of prostate cancer with long non-coding RNA-mediated competitive endogenous RNA network. Exp. Ther. Med. *17*, 3035–3040.

16. Zhao, Q., and Fan, C. (2019). A novel risk score system for assessment of ovarian cancer based on co-expression network analysis and expression level of five lncRNAs. BMC Med. Genet. *20*, 103–103.

17. Liu, Y., Feng, W., Liu, W., Kong, X., Li, L., He, J., Wang, D., Zhang, M., Zhou, G., Xu, W., et al. (2019). Circulating lncRNA ABHD11-AS1 serves as a biomarker for early pancreatic cancer diagnosis. J. Cancer *10*, 3746–3756.

18. Hara, T., Nakamura, K., Matsui, M., Yamamoto, A., Nakahara, Y., Suzuki-Migishima, R., Yokoyama, M., Mishima, K., Saito, I., Okano, H., and Mizushima, N. (2006). Suppression of basal autophagy in neural cells causes neurodegenerative disease in mice. Nature *441*, 885–889.

19. Levine, B., and Klionsky, D.J. (2004). Development by self-digestion: molecular mechanisms and biological functions of autophagy. Dev. Cell *6*, 463–477.

20. Yang, S., Wang, X., Contino, G., Liesa, M., Sahin, E., Ying, H., Bause, A., Li, Y., Stommel, J.M., Dell'antonio, G., et al. (2011). Pancreatic cancers require autophagy for tumor growth. Genes Dev. *25*, 717–729.

21. Guo, J.Y., Chen, H.-Y., Mathew, R., Fan, J., Strohecker, A.M., Karsli-Uzunbas, G., Kamphorst, J.J., Chen, G., Lemons, J.M., Karantza, V., et al. (2011). Activated Ras requires autophagy to maintain oxidative metabolism and tumorigenesis. Genes Dev. *25*, 460–470.

22. Karsli-Uzunbas, G., Guo, J.Y., Price, S., Teng, X., Laddha, S.V., Khor, S., Kalaany, N.Y., Jacks, T., Chan, C.S., Rabinowitz, J.D., and White, E. (2014). Autophagy is required for glucose homeostasis and lung tumor maintenance. Cancer Discov. *4*, 914–927.

23. Xie, X., Koh, J.Y., Price, S., White, E., and Mehnert, J.M. (2015). *Atg7* overcomes senescence and promotes growth of $Braf^{V600E}$-driven melanoma. Cancer Discov. *5*, 410–423.

24. Degenhardt, K., Mathew, R., Beaudoin, B., Bray, K., Anderson, D., Chen, G., Mukherjee, C., Shi, Y., Gélinas, C., Fan, Y., et al. (2006). Autophagy promotes tumor cell survival and restricts necrosis, inflammation, and tumorigenesis. Cancer Cell *10*, 51–64.

25. Mathew, R., Kongara, S., Beaudoin, B., Karp, C.M., Bray, K., Degenhardt, K., Chen, G., Jin, S., and White, E. (2007). Autophagy suppresses tumor progression by limiting chromosomal instability. Genes Dev. *21*, 1367–1381.

26. Lum, J.J., Bauer, D.E., Kong, M., Harris, M.H., Li, C., Lindsten, T., and Thompson, C.B. (2005). Growth factor regulation of autophagy and cell survival in the absence of apoptosis. Cell *120*, 237–248.

27. Karantza-Wadsworth, V., Patel, S., Kravchuk, O., Chen, G., Mathew, R., Jin, S., and White, E. (2007). Autophagy mitigates metabolic stress and genome damage in mammary tumorigenesis. Genes Dev. *21*, 1621–1635.

28. Karantza-Wadsworth, V., and White, E. (2007). Role of autophagy in breast cancer. Autophagy *3*, 610–613.

29. Mowers, E.E., Sharifi, M.N., and Macleod, K.F. (2017). Autophagy in cancer metastasis. Oncogene *36*, 1619–1630.

30. Zhan, Z., Li, Q., Wu, P., Ye, Y., Tseng, H.Y., Zhang, L., and Zhang, X.D. (2012). Autophagy-mediated HMGB1 release antagonizes apoptosis of gastric cancer cells induced by vincristine via transcriptional regulation of Mcl-1. Autophagy *8*, 109–121.

31. Kong, P., Zhu, X., Geng, Q., Xia, L., Sun, X., Chen, Y., Li, W., Zhou, Z., Zhan, Y., Xu, D., et al. (2017). The microRNA-423-3p-Bim axis promotes cancer progression and activates oncogenic autophagy in gastric cancer. Mol. Ther. *25*, 1027–1037.

32. Zhang, M., Weng, W., Zhang, Q., Wu, Y., Ni, S., Tan, C., Xu, M., Sun, H., Liu, C., Wei, P., and Du, X. (2018). The lncRNA NEAT1 activates Wnt/β-catenin signaling and promotes colorectal cancer progression via interacting with DDX5. J. Hematol. Oncol. *11*, 113.

33. Li, Y., Xiao, Y., Lin, H.P., Reichel, D., Bae, Y., Lee, E.Y., Jiang, Y., Huang, X., Yang, C., and Wang, Z. (2019). In vivo β-catenin attenuation by the integrin α5-targeting nano-delivery strategy suppresses triple negative breast cancer stemness and metastasis. Biomaterials *188*, 160–172.

34. Wang, L., Yu, T., Li, W., Li, M., Zuo, Q., Zou, Q., and Xiao, B. (2019). The miR-29c-KIAA1199 axis regulates gastric cancer migration by binding with WBP11 and PTP4A3. Oncogene *38*, 3134–3150.

35. Lu, F.-I., Sun, Y.-H., Wei, C.-Y., Thisse, C., and Thisse, B. (2014). Tissue-specific derepression of TCF/LEF controls the activity of the Wnt/β-catenin pathway. Nat. Commun. *5*, 5368.

36. Moon, R.T., Kohn, A.D., De Ferrari, G.V., and Kaykas, A. (2004). WNT and β-catenin signalling: diseases and therapies. Nat. Rev. Genet. *5*, 691–701.

37. Ji, C., Yang, L., Yi, W., Xiang, D., Wang, Y., Zhou, Z., Qian, F., Ren, Y., Cui, W., Zhang, X., et al. (2018). Capillary morphogenesis gene 2 maintains gastric cancer stem-like cell phenotype by activating a Wnt/β-catenin pathway. Oncogene *37*, 3953–3966.

38. Huang, J., Xiao, D., Li, G., Ma, J., Chen, P., Yuan, W., Hou, F., Ge, J., Zhong, M., Tang, Y., et al. (2014). EphA2 promotes epithelial-mesenchymal transition through the Wnt/β-catenin pathway in gastric cancer cells. Oncogene *33*, 2737–2747.

39. Clarke, M.F., and Fuller, M. (2006). Stem cells and cancer: two faces of eve. Cell *124*, 1111–1115.

40. Tirino, V., Desiderio, V., Paino, F., De Rosa, A., Papaccio, F., La Noce, M., Laino, L., De Francesco, F., and Papaccio, G. (2013). Cancer stem cells in solid tumors: an overview and new approaches for their isolation and characterization. FASEB J. *27*, 13–24.

41. Khan, S.A., Tyagi, M., Sharma, A.K., Barreto, S.G., Sirohi, B., Ramadwar, M., Shrikhande, S.V., and Gupta, S. (2014). Cell-type specificity of β-actin expression and its clinicopathological correlation in gastric adenocarcinoma. World J. Gastroenterol. *20*, 12202–12211.

42. Xu, J., Zhang, Z., Chen, J., Liu, F., and Bai, L. (2013). Overexpression of β-actin is closely associated with metastasis of gastric cancer. Hepatogastroenterology *60*, 620–623.

43. Mak, C.S.L., Yung, M.M.H., Hui, L.M.N., Leung, L.L., Liang, R., Chen, K., Liu, S.S., Qin, Y., Leung, T.H., Lee, K.F., et al. (2017). MicroRNA-141 enhances anoikis resistance in metastatic progression of ovarian cancer through targeting KLF12/Sp1/survivin axis. Mol. Cancer *16*, 11.

44. Phillips, C.M., Zatarain, J.R., Nicholls, M.E., Porter, C., Widen, S.G., Thanki, K., Johnson, P., Jawad, M.U., Moyer, M.P., Randall, J.W., et al. (2017). Upregulation of cystathionine-β-synthase in colonic epithelia reprograms metabolism and promotes carcinogenesis. Cancer Res. *77*, 5741–5754.

45. Haemmerle, M., Taylor, M.L., Gutschner, T., Pradeep, S., Cho, M.S., Sheng, J., Lyons, Y.M., Nagaraja, A.S., Dood, R.L., Wen, Y., et al. (2017). Platelets reduce anoikis and promote metastasis by activating YAP1 signaling. Nat. Commun. *8*, 310.

46. Reginato, M.J., Mills, K.R., Paulus, J.K., Lynch, D.K., Sgroi, D.C., Debnath, J., Muthuswamy, S.K., and Brugge, J.S. (2003). Integrins and EGFR coordinately regulate the pro-apoptotic protein Bim to prevent anoikis. Nat. Cell Biol. *5*, 733–740.

47. Mathew, R., Karantza-Wadsworth, V., and White, E. (2007). Role of autophagy in cancer. Nat. Rev. Cancer *7*, 961–967.

48. Levine, B., and Kroemer, G. (2008). Autophagy in the pathogenesis of disease. Cell *132*, 27–42.

49. Han, F., Li, C.F., Cai, Z., Zhang, X., Jin, G., Zhang, W.N., Xu, C., Wang, C.Y., Morrow, J., Zhang, S., et al. (2018). The critical role of AMPK in driving Akt activation under stress, tumorigenesis and drug resistance. Nat. Commun. *9*, 4728.

50. Mi, Y., Zhang, D., Jiang, W., Weng, J., Zhou, C., Huang, K., Tang, H., Yu, Y., Liu, X., Cui, W., et al. (2016). miR-181a-5p promotes the progression of gastric cancer via RASSF6-mediated MAPK signalling activation. Cancer Lett. *28*, 11–22.

51. Ohta, M., Tateishi, K., Kanai, F., Watabe, H., Kondo, S., Guleng, B., Tanaka, Y., Asaoka, Y., Jazag, A., Imamura, J., et al. (2005). p53-Independent negative regulation of p21/cyclin-dependent kinase-interacting protein 1 by the sonic hedgehog-glioma-associated oncogene 1 pathway in gastric carcinoma cells. Cancer Res. *65*, 10822–10829.

52. Bronte-Tinkew, D.M., Terebiznik, M., Franco, A., Ang, M., Ahn, D., Mimuro, H., Sasakawa, C., Ropeleski, M.J., Peek, R.M., Jr., and Jones, N.L. (2009). *Helicobacter pylori* cytotoxin-associated gene A activates the signal transducer and activator of transcription 3 pathway in vitro and in vivo. Cancer Res. *69*, 632–639.

53. Angers, S., and Moon, R.T. (2009). Proximal events in Wnt signal transduction. Nat. Rev. Mol. Cell Biol. *10*, 468–477.

54. Clark, M.B., and Mattick, J.S. (2011). Long noncoding RNAs in cell biology. Semin. Cell Dev. Biol. *22*, 366–376.

55. Tian, T., Lv, X., Pan, G., Lu, Y., Chen, W., He, W., Lei, X., Zhang, H., Liu, M., Sun, S., et al. (2019). Long noncoding RNA MPRL promotes mitochondrial fission and cisplatin chemosensitivity via disruption of pre-miRNA processing. Clin. Cancer Res. *25*, 3673–3688.

56. Fareh, M., Yeom, K.-H., Haagsma, A.C., Chauhan, S., Heo, I., and Joo, C. (2016). TRBP ensures efficient Dicer processing of precursor microRNA in RNA-crowded environments. Nat. Commun. *7*, 13694–13694.

57. Starega-Roslan, J., Galka-Marciniak, P., and Krzyzosiak, W.J. (2015). Nucleotide sequence of miRNA precursor contributes to cleavage site selection by Dicer. Nucleic Acids Res. *43*, 10939–10951.

58. Wu, D., and Pan, W. (2010). GSK3: a multifaceted kinase in Wnt signaling. Trends Biochem. Sci. *35*, 161–168.

59. Hannah, J., and Zhou, P. (2015). Distinct and overlapping functions of the cullin E3 ligase scaffolding proteins CUL4A and CUL4B. Gene *573*, 33–45.

60. Ni, W., Zhang, Y., Zhan, Z., Ye, F., Liang, Y., Huang, J., Chen, K., Chen, L., and Ding, Y. (2017). A novel lncRNA uc.134 represses hepatocellular carcinoma progression by inhibiting CUL4A-mediated ubiquitination of LATS1. J. Hematol. Oncol. *10*, 91.

61. Zhao, C., Deng, Y., Liu, L., Yu, K., Zhang, L., Wang, H., He, X., Wang, J., Lu, C., Wu, L.N., et al. (2016). Dual regulatory switch through interactions of Tcf7l2/Tcf4 with stage-specific partners propels oligodendroglial maturation. Nat. Commun. *7*, 10883.

62. Hrckulak, D., Kolar, M., Strnad, H., and Korinek, V. (2016). TCF/LEF transcription factors: an update from the internet resources. Cancers (Basel) *8*, 70.

63. Long, M., and McWilliams, T.G. (2020). Monitoring autophagy in cancer: from bench to bedside. Semin. Cancer Biol. *66*, 12–21.

64. Mizushima, N., Kuma, A., Kobayashi, Y., Yamamoto, A., Matsubae, M., Takao, T., Natsume, T., Ohsumi, Y., and Yoshimori, T. (2003). Mouse Apg16L, a novel WD-repeat protein, targets to the autophagic isolation membrane with the Apg12-Apg5 conjugate. J. Cell Sci. *116*, 1679–1688.

65. Mizushima, N., Yamamoto, A., Hatano, M., Kobayashi, Y., Kabeya, Y., Suzuki, K., Tokuhisa, T., Ohsumi, Y., and Yoshimori, T. (2001). Dissection of autophagosome formation using Apg5-deficient mouse embryonic stem cells. J. Cell Biol. *152*, 657–668.

66. Xu, Z., Li, Z., Wang, W., Xia, Y., He, Z., Li, B., Wang, S., Huang, X., Sun, G., Xu, J., et al. (2019). miR-1265 regulates cellular proliferation and apoptosis by targeting calcium binding protein 39 in gastric cancer and, thereby, impairing oncogenic autophagy. Cancer Lett. *449*, 226–236.

67. Tanida, I., Ueno, T., and Kominami, E. (2008). LC3 and autophagy. In Autophagosome and Phagosome, V. Deretic, ed. (Humana Press), pp. 77–88.

68. Loos, F., Xie, W., Sica, V., Bravo-San Pedro, J.M., Souquère, S., Pierron, G., Lachkar, S., Sauvat, A., Petrazzuolo, A., Jimenez, A.J., et al. (2019). Artificial tethering of LC3 or p62 to organelles is not sufficient to trigger autophagy. Cell Death Dis. *10*, 771.

69. Sánchez, Y., and Huarte, M. (2013). Long non-coding RNAs: challenges for diagnosis and therapies. Nucleic Acid Ther. *23*, 15–20.

70. Baehrecke, E.H. (2005). Autophagy: dual roles in life and death? Nat. Rev. Mol. Cell Biol. *6*, 505–510.

71. Wang, C., Tan, C., Wen, Y., Zhang, D., Li, G., Chang, L., Su, J., and Wang, X. (2019). FOXP1-induced lncRNA CLRN1-AS1 acts as a tumor suppressor in pituitary prolactinoma by repressing the autophagy via inactivating Wnt/β-catenin signaling pathway. Cell Death Dis. *10*, 499.

72. Nàger, M., Sallán, M.C., Visa, A., Pushparaj, C., Santacana, M., Macià, A., Yeramian, A., Cantí, C., and Herreros, J. (2018). Inhibition of WNT-CTNNB1 signaling upregulates SQSTM1 and sensitizes glioblastoma cells to autophagy blockers. Autophagy *14*, 619–636.

73. Petherick, K.J., Williams, A.C., Lane, J.D., Ordóñez-Morán, P., Huelsken, J., Collard, T.J., Smartt, H.J., Batson, J., Malik, K., Paraskeva, C., and Greenhough, A. (2013). Autolysosomal β-catenin degradation regulates Wnt-autophagy-p62 crosstalk. EMBO J. *32*, 1903–1916.

74. Zhang, H., Hua, Y., Jiang, Z., Yue, J., Shi, M., Zhen, X., Zhang, X., Yang, L., Zhou, R., and Wu, S. (2019). Cancer-associated fibroblast-promoted lncRNA *DNM3OS* confers radioresistance by regulating DNA damage response in esophageal squamous cell carcinoma. Clin. Cancer Res. *25*, 1989–2000.

75. Xie, M., Ma, T., Xue, J., Ma, H., Sun, M., Zhang, Z., Liu, M., Liu, Y., Ju, S., Wang, Z., and De, W. (2019). The long intergenic non-protein coding RNA 707 promotes proliferation and metastasis of gastric cancer by interacting with mRNA stabilizing protein HuR. Cancer Lett. *443*, 67–79.

76. Hu, X., Wang, Y., Liang, H., Fan, Q., Zhu, R., Cui, J., Zhang, W., Zen, K., Zhang, C.Y., Hou, D., et al. (2017). miR-23a/b promote tumor growth and suppress apoptosis by targeting PDCD4 in gastric cancer. Cell Death Dis. *8*, e3059.

77. Chen, Z., de Paiva, C.S., Luo, L., Kretzer, F.L., Pflugfelder, S.C., and Li, D.Q. (2004). Characterization of putative stem cell phenotype in human limbal epithelia. Stem Cells *22*, 355–366.

78. Xu, T.P., Liu, X.X., Xia, R., Yin, L., Kong, R., Chen, W.M., Huang, M.D., and Shu, Y.Q. (2015). SP1-induced upregulation of the long noncoding RNA *TINCR* regulates cell proliferation and apoptosis by affecting *KLF2* mRNA stability in gastric cancer. Oncogene *34*, 5648–5661.

79. Cho, K.O., Kim, J.Y., Jeong, K.H., Lee, M.Y., and Kim, S.Y. (2019). Increased expression of vascular endothelial growth factor-C and vascular endothelial growth factor receptor-3 after pilocarpine-induced status epilepticus in mice. Korean J. Physiol. Pharmacol. *23*, 281–289.

80. Xia, L., Liu, J., Sun, Y., Shi, H., Yang, G., Feng, Y., and Yin, S. (2019). Rosiglitazone improves glucocorticoid resistance in a sudden sensorineural hearing loss by promoting MAP kinase phosphatase-1 expression. Mediators Inflamm. *2019*, 7915730.